Document Number**:** H2020-ICT-52/RISE-6G/D4.2

Project Name:
Reconfigurable **I**ntelligent **S**ustainable **E**nvironments for **6G** Wireless Networks (RISE-6G)

Deliverable 4.2

Multi-user techniques and connectivity of RIS based communication and mobile edge computing (Intermediary Specifications)

Date of delivery:	30/06/2022	Version:	1.0
Start date of Project:	01/01/2021	Duration:	36 months

Deliverable D4.2
Multi-user techniques and connectivity of RIS based communication and mobile edge computing (Intermediary Specifications)

Project Number:	H2020-ICT-52 / 101017011
Project Name:	**R**econfigurable **I**ntelligent **S**ustainable **E**nvironments for **6G** Wireless Networks

Document Number:	H2020-ICT-52/RISE-6G/D4.2
Document Title:	Multi-user techniques and connectivity of RIS based communication and mobile edge computing (Intermediary Specifications)
Editor(s):	Marco Di Renzo (CNRS) and Fabio Saggese (AAU)
Authors:	Placido Mursia (NEC), Francesco Devoti (NEC), Paolo Di Lorenzo (CNIT), Sergio Barbarossa (CNIT), Marco Di Renzo (CNRS), Fatima Ezzahra Airod (CEA), Emilio Calvanese Strinati (CEA), Kyriakos Stylianopoulos (NKUA), George Alexandopoulos (NKUA)
Dissemination Level:	PU
Contractual Date of Delivery:	30/06/2022
Security:	Public
Status:	Final
Version:	1.2
File Name:	RISE-6G_D4.2_Final.docx

Abstract

This deliverable provides the results of the RISE-6G proposals on multi-user techniques for RIS-aided communication to work package 4 “RIS for Enhanced Connectivity and Reliability”, as well as initial performance evaluations of these proposals.

Keywords

Beyond-5G; 6G; RIS; Multi-user; Connectivity; Channel estimation; RIS-profile optimization; Edge computing

Contents

Figures

List of Acronyms

2D	two-dimensional
3D	three-dimensional
5G	5th Generation
A2G	Air-to-ground
AoA	Angle of arrival
AP	Access Point
BCD	Block coordinate descent
BER	Bit Error Rate
BS	Base station
CDF	Cumulative density function
CPU	Central processing unit
CSIT	Channel state information at the transmitter
DDPG	Deep Deterministic Policy Gradient
DEA	Dynamical energy analysis
DL	Downlink
DOF	Degree of freedom
DQN	Deep Q Networks
DRL	Deep Reinforcement Learning
E2E	End-to-End
EE	Energy Efficiency
EM	Electromagnetic
ES	Edge server
GHz	Giga-Hertz
HRIS	Hybrid RIS
IoT	Internet of Things
KPI	Key performance indicator
LIS	Large intelligent surface
LoS	Line of Sight
MEC	Mobile Edge Computing
MIMO	Multiple-input multiple-output
MMSE	Minimum mean squared error
MRT	Maximum ration transmission

MSE	Mean Squared Error
NLoS	Non-line-of-sight
NMSE	Normalized Mean Squared Error
PEC	perfect electric conductor
PIN	positive-intrinsic-negative
PL	Physical Layer
RAT	Radio access technology
RCS	Radar cross section
RF	Radio frequency
RIS	Reconfigurable intelligent surface
RISC	RIS controller
RISE	RIS enabled
RL	Reinforcement Learning
SDR	Semidefinite relaxation
SE	Spectral Efficiency
SINR	Signal to Interference plus Noise Ratio
SLNR	Signal to leakage and noise ratio
SMSE	Sum mean squared error
SNR	Signal to Noise Ratio
SotA	State-of-the-art
THz	Tera-Hertz
UAV	Unmanned Aerial Vehicle
UE	User equipment
wMMSE	Weighted mean squared error
ZF	Zero-forcing

List of Tables

1 Introduction

In the present deliverable, we report the research work carried out by the consortium of RISE-6G on multi-user algorithms and protocols for application to RIS-aided smart radio environments. The research findings reported in the present deliverable are in agreement with the initial specifications reported in deliverable D4.1 titled “On deployment and control strategies of RIS based connectivity”. The results reported in the present deliverable constitute initial specifications that will be further elaborated and finalized in deliverable D4.4.

1.1 Deliverable objectives

The objectives of the present deliverable are the following:

(1) To report specifications and intermediate results on fundamental performance limits in RIS-aided smart radio environments, which account for RIS-aided channel models and the associated control overhead.

(2) To report specifications and intermediate results on the design and optimisation of control signalling protocols, channel estimation algorithms, and resource allocation and scheduling policies to support the efficient deployment of RISs in smart radio environments.

(3) To report specifications and intermediate results on the design and optimisation of resilient, energy efficient, and joint communication and computation mechanisms with low electromagnetic field exposure for application to power- and latency-constrained (edge) cloud services.

1.2 Deliverable structure

After reviewing the key performance metrics and KPI specified in deliverable D4.1, which drives the development of the research work within WP4 and the RISE-6G project, the present deliverable is logically organized in compliance with the tasks of WP4. More specifically, deliverable D4.2 is organized in three main macro sections that are focused on:

(1) The fundamentals of multi-user network connectivity for RISE systems

(2) The design of multi-user techniques for RISE communications

(3) The design of multi-user techniques for RIS-empowered mobile edge computing

In this document, multi-user can refer also to multi-RIS, systems which requires coordination techniques as well. Moreover, we remark that with RISE system we refer to every kind of network including RISs, while with “RIS-empowered” or “RIS-aided” we refer to systems where a single or multiple RISs are used to enhance the achievable performance.

As far as the first macro section is concerned, we report seven main research and technology contributions made by the RISE-6G consortium, listed as follows: (i) design of efficient beamforming schemes for application to RIS-aided IoT massive access; (ii) design of RIS-aided robust and reliable air-to-ground communication networks enabled by UAVs; (iii) design of frequency-agnostic control schemes for smart radio environments: (iv) design of self-configuring RISs with reduced control channel requirements; (v) design of efficient optimization methods based on quantum annealing; (vi) design of efficient optimization methods based on electromagnetic-consistent models for RISs; (vii) analysis of the degrees of freedom of RIS-aided channels based on ray tracing methods; and (viii) development of a frequency mixing architecture for RIS-aided nonlinear wireless channels.

As far as the second macro section is concerned, we report seven main scientific contributions made by the RISE-6G consortium, listed as follows: (i) design of tensor-based channel tracking methods for RIS-aided multi-user channels; (ii) design of optimization methods for sum-rate optimization that rely on statistical channel state information for reducing the overhead; (iii) concept and design of random access protocols based on beam sweeping methods; (iv) design of efficient orchestration algorithms for system optimization based on reinforcement learning methods; (v) optimization of RISs based on supervised learning methods and the users' locations; (vi) design of multi-beamforming algorithms to enable the reconfigurability at the physical layer.

As far as the third macro section is concerned, we report four main scientific contributions made by the RISE-6G consortium as the following (i) joint optimization and scheduling of MEC-aided communication and computation tasks; (ii) design of MEC-aided schemes for application to RIS-assisted wireless links in the millimetre-wave frequency band; (iii) design of adaptive federated learning schemes for smart radio environments; and (iv) design of dynamic computation offloading methods for application to frequency-selective RIS-aided channels.

Finally, the present deliverable is concluded with a summary of the main obtained scientific contributions.

1.3 Definitions and taxonomy

The main notation symbols appearing throughout the document are listed in Table 1-1. Miscellaneous self-contained notation introduced in certain contributions will be defined per case. In listed figures and algorithms, the notation may follow that of the corresponding publication, for a more consistent presentation.

Table 1-1: Definition of the main notation symbols.

Parameter	Notation	Parameter	Notation	Parameter	Notation
Total number of UEs	K	Receive signal at UE k	y_k	Transmit symbol for UE k	s_k
RIS phase shift matrix	$\boldsymbol{\Phi}$	Number of RIS elements	$N = N_x \times N_y$	BS precoder	$\boldsymbol{v}$
Power budget at the BS	P	Working wavelength	λ	Receiver noise	n_k
Sum rate	R_{tot}	Rate of UE k	R_k	Working frequency	f

2 Metrics and KPIs

This section introduces the KPIs that are relevant for quantifying the performance for RIS-empowered multi-user connectivity and edge-computing. The metrics have been introduced in D4.1, and are repeated here for the purpose of presenting a self-contained document. There is a close correspondence with what is described in Deliverables D2.2 and D2.4 of this project which concern the general KPI definitions. However, this document includes a more detailed description of the metrics specifically relevant to WP4 and the algorithmic methodologies to be presented.

The metrics presented below constitute ubiquitous performance indicators in wireless communications, which, in most cases, have been redefined or extended to account for the introduction of the RIS in the communication system.

2.1 Latency

In a communications system, ***latency*** expresses the time delay between the initiation of an event and the actuation of its effect. It is one of the key performance metrics in current and next-generation communications. Indeed, 6G specifications target end-to-end (E2E) latency objective of up to 10μs [GRT21]. From a wireless system engineering perspective, we consider the Physical Layer (PL) latency, which is given by the sum of the following components [XH21]:

$$T_{PL} = T_{que} + T_{ttt} + T_{proc} + T_{prop} + T_{retr}$$

where

- T_{que} is the queueing latency arising from the waiting time of the current packet until the transmission of the previous packet is completed.
- T_{ttt} (time-to-transmission) is the time needed for the packet to be forwarded to the physical link.
- T_{proc} denotes the processing latency, which accounts for the operations applied to the transmitted data (e.g., encoding/decoding, precoding/combining, modulation/demodulation, channel interleaving and estimation, scrambling, data and control multiplexing).
- T_{pro} expresses the propagation time of the electromagnetic waves takes to reach the destination.
- T_{retr} captures the delay induced by retransmissions in case of packet loss and is, generally, a function proportional to the number of retransmissions, T_{proc} and T_{prop}.

In the context of RIS-based connectivity, the T_{proc} component is of particular interest since it is directly affected by the deployment and control strategies adopted. We remark that the channel estimation processing and the optimization of the RIS configuration may not be needed to forward the packet to the physical link. As a results, these processes (or a part of them) can be performed in parallel, reducing *de facto* the overall time T_{proc}.

Furthermore, depending on the system under examination, specific sub-components of the processing latency can be defined. In the sequel, we also highlight the latency in the MEC context, which depends on the nature of the computation offloading. Since operations involving MEC consider a more elaborate system, we consider the definition of the E2E latency, which is a more general definition than the PL latency given above. In particular, the delays associated with the physical layer operations are captured in the UL and DL communication times, as defined below.

Static computation offloading

Static computation offloading deals with brief time applications, where mobile users send a single computation request, typically also specifying a service time. Let $A_k(t)$ be the number of input bits required by the application run by user k at time t, and let $w_k(t)$ be the number of CPU cycles associated with the computing task. Then, the overall E2E latency of UE k is composed of three terms: (i) an UL communication time $\Delta_k^u(t)$, needed by the device to send the input bits to the BS; (ii) a computation time $\Delta_k^c(t)$, needed by the Edge Server (ES) to process the input bits and run the specific application; (iii) a DL communication time $\Delta_k^d(t)$,

needed by the BS to send the result of computation back to the UE(s). In summary, the overall E2E latency at time t is given by:

$$\Delta_k(t) = \Delta_k^u(t) + \Delta_k^c(t) + \Delta_k^d(t) = \frac{A_k(t)}{R_k(t)} + \frac{w_k(t)}{f_k(t)} + \frac{B_k(t)}{R_k^d(t)}$$

where $R_k(t)$ is the uplink rate from UE k to the BS, $f_k(t)$ is the CPU frequency allocated by the edge server to UE k, $R_k^d(t)$ is the downlink rate from the BS to UE k, and $B_k(t)$ is the number of output bits of the application run by the ES on behalf of UE k. In static computation offloading, communication and computation resources are orchestrated to guarantee that the overall E2E delay $\Delta_k(t)$ is less than or equal to an application-dependent requirement, say L_k for all t.

Dynamic computation offloading

In *dynamic computation offloading,* each device continuously generates data $A_k(t)$ to be processed (e.g., the transmission of a video recorded by a UE to be processed by the ES for pattern recognition or anomaly detection). Then, a queueing system is used to model and control the dynamic data generation, transmission, and processing. At each time slot t, each user buffers data in a local queue $Q_k^l(t)$ and transmits them to the AP at the transmission rate $R_k(t)$. The local queue update follows the rule:

$$Q_k^l(t+1) = max\left(0, Q_k^l(t) - \tau R_k(t)\right) + A_k(t)$$

where τ is the duration of the time-slot used for scheduling the resources.

Then, the BS receives data from each device k and sends the data to the ES, which processes J_k bits-per-cycle, where J_k is a parameter that depends on the application offloaded by device k. Thus, the computation queue at the ES evolves as:

$$Q_k^c(t+1) = \max(0, Q_k^c(t) - \tau f_k(t) J_k) + \min(Q_k^l(t), \tau R_k(t))$$

Finally, the BS sends back to each user the bits resulting from the computation, draining a downlink communication queue that evolves as:

$$Q_k^d(t+1) = \max\left(0, Q_k^d(t) - \tau R_k^d(t)\right) + c_k \min(Q_k^c(t), \tau f_k(t) J_k)$$

where c_k denotes the ratio between output and input bits of the application required by user k. Thus, the E2E delay experienced by offloaded data is related to the sum of the three queues

$$Q_k^{tot}(t) = Q_k^l(t) + Q_k^c(t) + Q_k^d(t).$$

From Little's law, given an average data arrival rate $\bar{A}_k = \mathbb{E}[A_k(t)]$, (where $\mathbb{E}[.]$ is the expectation) the average latency experienced by a new data unit from its generation to its computation at the ES is:

$$\bar{D}_k = \lim_{T\to\infty} \frac{1}{T} \sum_{t=1}^{T} \mathbb{E}\left[\frac{Q_k^{tot}(t)}{\bar{A}_k}\right].$$

Thus, in this dynamic context, an average E2E delay constraint can be written as:

$$\lim_{T\to\infty} \frac{1}{T} \sum_{t=1}^{T} \mathbb{E}[Q_k^{tot}(t)] \leq Q_k^{avg} = D_k^{avg} \bar{A}_k$$

More sophisticated probabilistic constraints can also be imposed on the maximum tolerable delay.

2.2 Spectral efficiency and throughput

In this sub-section, we provide an example of definition of the ***SE*** metric, which concerns the rate of reliably transmitted information over the allocated communication bandwidth B. The

central concept behind spectral efficiency is the (received) SNR which expresses the ratio between the power of the transmitted signal as it reaches the UE, over the power of the background noise. The presence of the RIS affects the received power of the end-to-end channel by reflecting the impinging EM waves so that they form beams of concentrated power to desired locations. For multi-user communications, this idea extends to the SINR, which also captures the interference signals appearing due to the simultaneous communication of multiple ends.
Formally, the achievable SE with respect to a UE depends on the UE's SINR. For instance, the achievable SE with respect to a UE *k* is given by

$$\mathbf{SE}_k = \log_2(1 + \mathbf{SINR}_k) \quad (\mathbf{bits/s/Hz})$$

and the *sum-rate over the allocated bandwidth* (i.e., the sum of individual rates for all UEs) reads as:

$$\mathcal{R} = \sum_k \mathbf{SE}_k$$

Finally, the throughput of the considered system is finally given by $\boldsymbol{T} = \boldsymbol{B\mathcal{R}}$.

2.3 Reliability

We define the notion of ***reliability*** of the communication by considering a given minimum SINR threshold denoted as θ, which is necessary to decode the incoming signal. We define the set of UEs whose received SINR is greater than θ as the following

$$\mathcal{U} = \{k : \mathbf{SINR}_k \geq \theta\}$$

RIS-enabled systems are expected to enlarge the network area in which the received SINR of a given UE is above a given threshold, and thus sufficient for successful decoding of the incoming signal.

2.4 Bit Error Rate and Bit Error Ratio

Considering a digital transmission, the BER defines the number of bits received incorrectly by the end node per unit time. The normalized version of this metric, the ***Bit Error Ratio*** concerns the number of incorrect bits as a proportion of the total number of bits transmitted.

2.5 Energy efficiency

The ***EE*** for a downlink communication from a BS to a UE is defined as follows:

$$EE = \mathcal{R}/\mathbf{P} \ (\mathbf{bits/s/Hz/Watt})$$

where $\mathcal{R}$ is the sum data spectral efficiency and P is the total power consumption, including the circuitry and the power used for transmission/reception.

2.6 Channel estimation accuracy

For the specific problem of channel estimation, we consider the ***NMSE*** to assess the performance of the estimation process. Specifically, NMSE (in dB) is defined as:

$$\mathbf{NMSE} = \mathbb{E}\left[10\log_{10}\frac{\left\|\mathbf{H} - \widehat{\mathbf{H}}\right\|_F^2}{\|\mathbf{H}\|_F^2}\right]$$

where $\mathbf{H}$ and $\widehat{\mathbf{H}}$ are the true and estimated channel matrices, respectively, and $\|\cdot\|_F$ is the Frobenius norm.

3 Fundamentals of Multi-User Network Connectivity for RISE Systems

3.1 Joint Active and Passive Beamforming

In this section, we give the most general definition of the multi-user problem in RIS-aided wireless networks. In particular, we show how the key aspect is the joint optimization of the (active) beamforming at the BS and the (passive) beamforming at the RIS. In the default settings, a given number of users K is scheduled to be served in the same time-frequency resources.

Focusing on the downlink, let y_k denote the received signal at the (single-antenna) UE k, which is defined as

$$y_k = (\boldsymbol{h}_k^H \boldsymbol{\Phi} \boldsymbol{G} + \boldsymbol{h}_{d,k}^H)\boldsymbol{v}\, s_k + n_k$$

where $\boldsymbol{h}_k^H$, $\boldsymbol{G}$, and $\boldsymbol{h}_{d,k}^H$ denote the channel vectors from the RIS to the UE, from the BS to the RIS and from the RIS to the UE, respectively, and all other notation are defined as in Section 2.1. Here, the BS precoder and the RIS phase-shifting matrix contribute together to the received signal quality. Hence, their optimization must be jointly considered. Let $f(\cdot)$ be the considered network utility function, such that we can define the following optimization problem

$$\begin{aligned} &\max_{\boldsymbol{\Phi},\boldsymbol{v}} f(\boldsymbol{\Phi},\boldsymbol{v}) \\ &\text{s.t.} \quad \left|[\boldsymbol{\Phi}]_{i,i}\right|^2 \leq 1, \qquad \left|[\boldsymbol{\Phi}]_{i,j}\right|^2 = 0 \\ &\qquad \|\boldsymbol{v}\|^2 \leq P \end{aligned}$$

where the first constraint is required to guarantee that the phase-shift configuration at the RIS is given by a diagonal matrix and that the incoming signal is not amplified, while the second constraint limits the transmit power at the BS.

In this regard, the choice of the objective function is of paramount importance, especially for massive access scenarios. Indeed, it must be chosen to provide high-performing solutions while guaranteeing efficiency and scalability. While several existing works focus on maximizing the rate of each UE (see, e.g., [WZ19]), which is a highly-challenging non-convex problem, in [MSG21] the SMSE of the received signal has been shown to have a convex structure in the two optimization variables separately, i.e., $\boldsymbol{\Phi}$ and $\boldsymbol{v}$. Note that in the most general definition of such problem, the RIS is treated as an *ideal* hardware capable of any continuous phase-shift. However, several existing works consider the more practical case of a discrete set of phase-shifting configurations.

The above-referenced signal model is based on conventional communication and antenna theory and assumes absence of mutual coupling (i.e., half-wavelength inter-element distance), far-field, and independence between the signal attenuation and phase shift at each RIS unit cell [HZA19]. Depending on the application environment and the available practical hardware, some of these assumptions may not hold in real-life scenarios. Moreover, accurate channel modelling, such as via the ray tracing methods outlined in Section 3.5.6, is of high importance to gain important insights and understandings on the achievable performance of RIS-aided networks.

In this regard, an electromagnetic-compliant and mutual coupling aware channel model was recently introduced in [GD21], which is equivalent to a MIMO channel. Under this setting, the above signal model is modified as follows (for the case of single-antenna transmitter)

$$y_k = H_{e2e}\, s_k + n_k$$

where the channel coefficient is given by

$$H_{e2e} = y_0(Z_{RT} - \boldsymbol{Z}_{RS}(\boldsymbol{Z}_{RIS} + \boldsymbol{Z}_{SS})^{-1}\boldsymbol{Z}_{ST}),$$

with y_0 accounting for internal impedance of the voltage generator of the transmitter, load impedance of the receiver, and self-impedance of the transmit and receive antennas, whereas $\boldsymbol{Z}_{X,Y}$ is the (self) mutual impedance between X and Y, where T, R, S stand for the transmitter, the receiver and the RIS, respectively. Moreover, $\boldsymbol{Z}_{RIS}$ represents the tunable (diagonal) impedance matrix at the RIS. Under this model, the optimization procedure requires to deal with the inverse operation, which further compounds the complexity of designing optimal RIS strategies [A21][QD21].

3.2 Static versus Nomadic RIS

In the previous section, we assumed a static RIS position, e.g., mounted on the façade of a building or indoor wall. However, this might not be the case for some novel RIS use cases.

In this regard, consider the newly-defined concept of air-to-ground network, whereby aerial devices, such as UAVs, are used to facilitate the communication between a BS and a set of target UEs by flying above obstacles and providing enhanced connection reliability. In this context, RISs can be leveraged to alleviate the limited battery life of such devices, while guaranteeing advanced beamforming capabilities.

Owing to the non-static RIS position, the aforementioned multi-user problem formulation is modified by introducing the variation of the RIS position and orientation over time [DMS22][PSZ21].

Moreover, since UAVs might be subject to unwanted perturbations caused by meteorological phenomena, the system needs to take into account a degree of uncertainty on the (nominal) position and orientation of the RIS [MDS21].

3.3 Exploiting the Frequency Domain in RISE Systems

While in Section 3.1, the problem of multi-user network connectivity in RISE systems is treated by designing optimized beamforming techniques both at the RIS and at the BS, advanced RIS hardware design may be exploited to achieve multi-frequency operation, without the need of redundant deployments.

Indeed, novel RIS designs allow to operate on different frequency bands with the same hardware. In this way, the users may be scheduled in the frequency-domain as well and/or multiple RATs may be supported. In [MAM22], the RIS unit cell is replaced by a reconfigurable patch-antenna, i.e., an antenna whose operating frequency may be dynamically configured. By doing so, and depending on the chosen working frequency, the inter-element spacing may be different than the conventional half-wavelength. As a result, the array response may be corrupted by mutual coupling effects. A solution to this problem may be given by selectively turning-off antenna elements, as to restore independence across the array of antennas. The choice of the elements activation requires additional optimization, which is coupled with the current propagation environment and application scenario.

Moreover, the frequency dimension can be exploited for reducing the overhead of the CSI estimation. The RIS design in [RSA20] **Erreur ! Source du renvoi introuvable.** is capable of manipulating the frequency of the incident signals. Such effect can be exploited to derive frequency-mixing operating RISs, whereby the narrowband transmitted signal is expanded in the frequency domain by creating additional paths that may lead to ideal i.i.d propagation environments. Since such paths are decoupled in the frequency domain, one single pilot is sufficient for channel estimation, as proven in [YDW21].

3.4 Autonomous RISs

The above-mentioned methods rely on a control channel between the BS and the RIS, which is used to communicate to the RISC the optimized phase-shift configuration. Moreover, the BS exploits the available CSIT to optimize the given network utility metric.

In real-life scenarios, such assumptions may be unpractical or even unfeasible. Hence, recent works have introduced the concept of self-configuring RISs, whereby the RISC exploits only locally-available CSI to automatically find the best RIS configuration.

In [ADS22], the authors propose to embed the RIS with basic sensing capabilities and denote it with *hybrid* RIS (HRIS). In particular, a fraction of the incident signal is redirected to a sensing branch on the RIS. Both signal components are phase-shifted by the same amount, which is different for each unit cell. During uplink transmission, the power of the signal obtained by summing-up all the outputs of sensing branches across the array can be exploited to infer the location of the intended receiver. Such information, together with the known BS position, is then exploited to self-configure the RIS by aligning it to the direction of maximum power as computed by the sensing branch.

3.5 Contributions from RISE-6G

The following table lists the relevant contributions from RISE-6G in the multi-user connectivity design for RISE systems and summarizes the key system parameters.

Table 3-1: Fundamentals of multi-user network connectivity: Contributions from RISE-6G.

Parameter	**A-0: Reconfigurable Intelligent Surfaces Enabling Beamforming for IoT Massive Access**	**A-1: RIS-Empowered UAV Communications for Robust and Reliable Air-to-Ground Networks**	**A-2: A Frequency-Agnostic RIS-based solution to control the Smart Radio Propagation Environment**	**A-3: A Self-Configuring RIS Solution Towards 6G**
Objective function	Minimize SMSE	Maximize minimum SNR	Maximize SLNR	Maximize rate
Optimization variables	RIS phase-shifts and BS precoder	RIS phase-shifts and BS precoder	RIS phase-shifts, activation profile, and BS precoder	RIS phase-shifts
CSI	Perfect	Statistical knowledge	Perfect	Unknown
#BS	1	1	1	1
#RIS	1	1	1	1
Continuous/quantized phase-shifting	Both	Continuous	Continuous	Continuous
Parameter	**A-4: Statistical mechanics methods for RIS optimization: Ising Hamiltonian and Quantum Annealing**	**A-5: Mutual Coupling Aware Sum-Rate Optimization of Reconfigurable Intelligent Surfaces Based on a Mutual**	**A-6: Degree-of-Freedom estimation from ray tracing**	**A-7: Frequency-Mixing RIS for Nonlinear Wireless Propagation**

		Impedance Channel Model		
Objective function	Maximize SNR	Maximize sum rate	Maximize Diversity Gain	Minimize number of pilot sent during channel estimation
Optimization variables	RIS phase-shifts	RIS tunable impedance matrix Precoding Matrix	Transmiting RIS basis functions, position and dimension	Continuous RIS phase-shifts
CSI	-	Perfect	Perfect	-
#BS	-	Multiple	1	1
#RIS	1	Multiple	1	1
Continuous/quantized phase-shifting	Quantized	Continuous	-	Continuous

3.5.1 Contribution #A-0: Reconfigurable Intelligent Surfaces Enabling Beamforming for IoT Massive Access

Motivation and context

We consider a beyond 5G massive access scenario in a heterogeneous IoT multi-UE cellular network consisting of a multi-antenna BS serving a large set of single-antenna UEs with the aid of an RIS to cope with NLoS paths [MSG21]. Figure 3-1 depicts the considered network where the number of UEs is large and there is no specific assumption on their hardware characteristics, ranging from cars to phones, tables, or wearables. In this context, we claim that active beamforming via an antenna array at the transmitter side and passive beamforming in the channel via a RIS can complement each other and provide even larger gains when they both are jointly optimized.

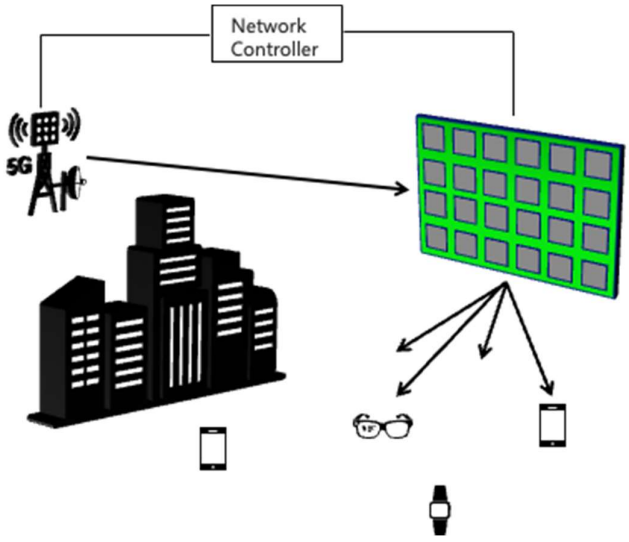

Figure 3-1: Heterogeneous beyond 5G IoT network

Specifically, we consider an M-antenna BS that wants to serve K single-antenna UEs with the aid of an N-element RIS. We further assume perfect CSIT, as to give a fundamental upper bound on the achievable performance of such a system.

Methodology

The main novelty of this contribution stems from exploiting the SMSE as an optimization objective. Given the receive signal $y_k \in \mathbb{C}$ at UE k and its corresponding transmit symbols $s_k \in \mathbb{C}$, the SMSE is given by

$$SMSE = \sum_{k=1}^{K} MSE_k$$

$$= \sum_{k=1}^{K} [\![E[|y_k - s_k|]\!]^2]$$

Interestingly, such metric reveals a convex structure in the two optimization variables separately, namely the precoding strategy at the transmitter and the RIS parameters. This allows to design very efficient iterative algorithms for RIS control. Specifically, we present RISMA, a RIS-aided Multiuser Alternating optimization algorithm that jointly optimizes the beamforming strategy at the transmitter (a BS) and the RIS parameters to provide high-bandwidth low-cost connectivity in massive IoT scenarios [MSG21].

It is important to highlight that the SMSE is not necessarily fair among the UEs, since it focuses on optimizing the overall system performance. Hence, UEs in good channel conditions will obtain a higher overall transmission rate.

Moreover, we adapt RISMA, which provides a solution from a theoretical perspective, to accommodate practical constraints when using low-resolution RISs that are comprised of antenna elements that can be activated in a binary fashion. In this way, these are RISs that only support phase shift values from a discrete set, rather than any real value from a range, and further compound our problem [HZD20], [DDC20]. To address this scenario, we propose Lo-RISMA, which decouples the optimization of the binary activation coefficients and the quantized phase shifts. The coefficients are optimized via SDR while the phase shifts are obtained by projecting the ideal continuous phases onto the given discrete space.

Results and outcomes

As depicted in Figure 3-2, the proposed RISMA approach outperforms conventional SotA approaches such as MMSE and ZF precoding (see [PHS05] and [SSH04], respectively). In particular, we demonstrate its performance in terms of achievable sum rate versus the number of BS antennas K and for increasing number of UEs K.

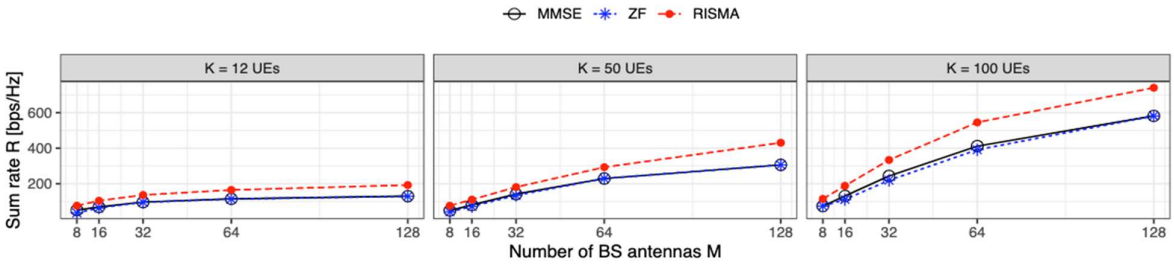

Figure 3-2: Sum rate performance of RISMA versus SotA techniques versus the number of BS antennas and for different values of number of UEs.

Perspective and relation to other WP4 contributions

This contribution provides an upper bound on the achievable performance in terms of system sum rate. Indeed, it considers the limit case of perfect CSIT and ideal RIS hardware. It can be used as performance benchmark by other contributions, which tackle practical scenarios and incorporate real-life constraints.

3.5.2 Contribution #A-1: RIS-Empowered UAV Communications for Robust and Reliable Air-to-Ground Networks

Motivation and context

We propose a novel optimization framework to provide robust and reliable air-to-ground networks by compensating for undesired *flight effects* such as variations of the position and orientation of the flying device due to adverse meteorological phenomena [MDS21]. Indeed, such unwanted perturbations result in instantaneously-wrong RIS configurations, which negatively impact the communication performance if not taken into account.

As depicted in Figure 3-3, we consider a network comprised of an M-antenna transmitter located at the origin of the 3D reference system, a planar $N_x \times N_y$- antenna RIS, where N_x and N_y are the number of elements along the x and y axis, respectively, mounted on-board a UAV, which is located in position $\boldsymbol{q} = [q_x \quad q_y \quad q_z]^T$ and a target area A wherein first responders and/or victims are present. Each intended receiver is located in position $\boldsymbol{w} = [w_x \quad w_y \quad w_z]^T$ and shall be reached with a sufficient SNR for successful decoding of the incoming signal. We further let θ_R (θ_T) denote the receive (transmit) elevation angle of arrival (departure) at the RIS and ϕ_R (ϕ_T) the receiver (transmit) azimuth angle of arrival (departure).

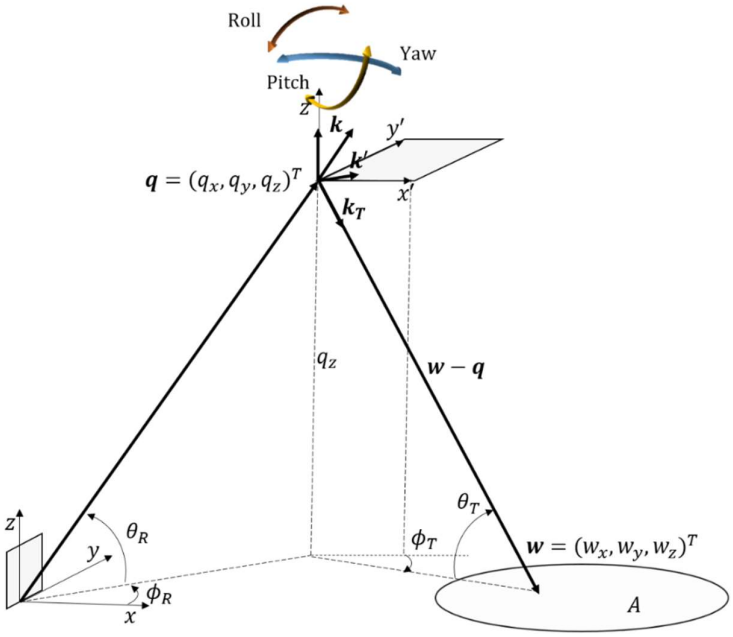

Figure 3-3: Considered A2G network system model.

The undesired roll, yaw and pitch of the surface of the RIS are modelled as mutually independent normally distributed random variables $\boldsymbol{r} = [\psi_x \quad \psi_y \quad \psi_z]^T$, with zero mean and given standard deviation σ_x, σ_y, and σ_z, respectively. Only the statistical properties of such unwanted perturbations are assumed to be known.

The target users are assumed to be distributed within the target area A with a given probability density function $f_W(\boldsymbol{w})$, which is assumed to be known.

Methodology

We study the problem of maximizing the worst SNR within the specified target area to be covered A, by suitably optimizing both the BS and RIS configurations for a given user statistical distribution and UAV perturbation statistics. Such optimization problem is formalized as follows

$$\begin{aligned} \max_{\boldsymbol{\Phi},\boldsymbol{v}} \ & \min_{\boldsymbol{w}\sim f_W(\boldsymbol{w})} \ \mathbb{E}[\mathrm{SNR}(\boldsymbol{q},\boldsymbol{w},\boldsymbol{r},\boldsymbol{\Phi},\boldsymbol{v})] \\ & s.t. \qquad \|\boldsymbol{v}\|^2 \le P; \\ & \qquad\quad [\boldsymbol{\Phi}]_{i,i} \le 1, \qquad [\boldsymbol{\Phi}]_{i,j} = 0 \end{aligned}$$

where the matrix $\boldsymbol{\Phi}$ contains the RIS beamforming configuration, the vector $\boldsymbol{v}$ contains the BS configuration, P is the power budget at the BS and the expectation operator allows us to design a statistical method that aims at counteracting on average the random fluctuations in the received SNR due to the unwanted UAV perturbations.

The above mentioned problem is non-convex and highly complex to tackle due to the generic form of the user pdf within the target area. Our proposed solution, namely *RiFe*, consists in firstly applying Monte Carlo sampling to draw N_w points from the given user distribution. If N_w is large enough, we obtain a correct sampling of the distribution, at the cost of increased complexity. We then fix the BS configuration as MRT to the (nominal) UAV-RIS position and we optimize the RIS configuration by applying SDR, which is followed by a rank-1 approximation via Gaussian randomization.

Results and outcomes

In Figure 3-4, we evaluate the CDF of the minimum SNR in the specified target area obtained with the proposed RiFe approach and an agnostic approach that does not take into account the statistics on the UAV perturbations versus the system SNR and for different values of the UAV perturbation statistics σ (note that for simplicity we assume $\sigma_x = \sigma_y = \sigma_z = \sigma$) and radius of the considered circular target area (2.5 m on the left-hand side and 10 m on the right-hand side).

Remarkably, our proposed approach manages to substantially increase the average minimum SNR in all the considered cases, especially under strong perturbations, thus guaranteeing an acceptable level of signal quality even under adverse atmospheric conditions.

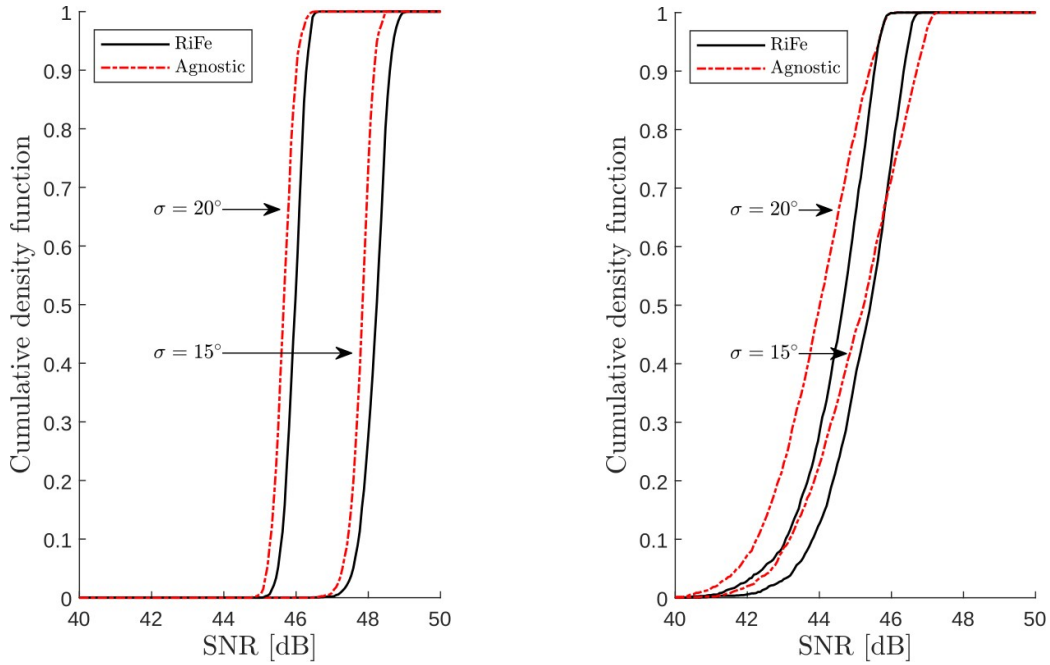

Figure 3-4: CDF of the proposed RiFe and the agnostic approach versus the SNR and for different values of UAV perturbations and victim spread (2.5 m on the left-hand side and 10 m on the right-hand side).

Perspective and relation to other WP4 contributions

This contribution proposed a RIS optimization technique that is suited for multi-UE scenarios where the only known CSI is the user distribution in space. It may be enhanced by incorporating more advanced joint BS and RIS beamforming optimization techniques, or by endowing the RIS on-board the UAV with self-configuring capabilities.

3.5.3 Contribution #A-2: A Frequency-Agnostic RIS-based solution to control the Smart Radio Propagation Environment

Motivation and context

In [MAM22] we propose a novel multi-frequency RIS design to dynamically operate between different radio frequencies without having to change the RIS hardware, which is based on reconfigurable patch antennas and PIN diodes. In particular, as depicted in Figure 3-5, our proposed unit cell is made of a two-layer patch antenna, where the inner layer is designed to work at 27.96 GHz (with the outer layer disabled), while the union of both layers resonates at 21.28 GHz. Such layers are connected via a PIN diode, which selectively activates the outer layer and is modelled in CST Studio Suite® via two PEC pads. The performance of such novel unit cell RIS design in terms of scattering parameters is shown in Figure 3-6.

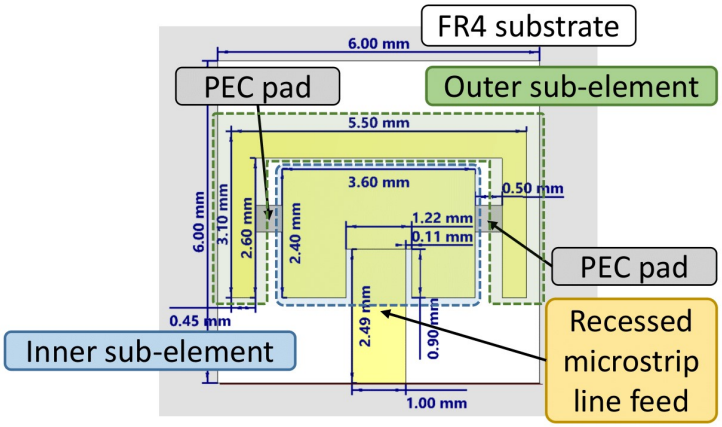

Figure 3-5: CST model of the proposed muti-frequency RIS unit cell.

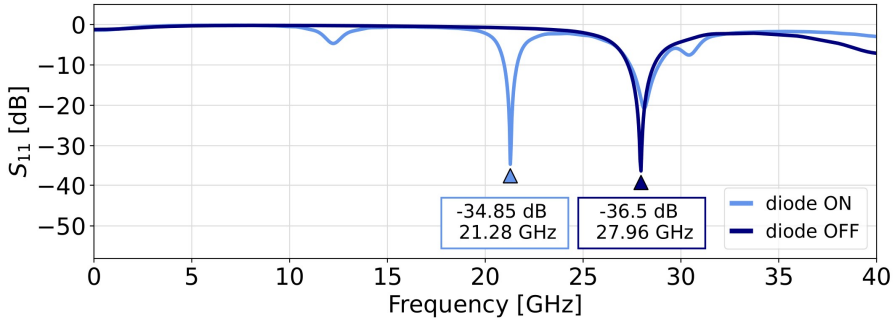

Figure 3-6: Full-wave simulation in CST of a single multi-frequency RIS unit cell in terms of scattering parameters.

Since the RIS hardware is fixed, when operating at the two different radio frequencies the inter-element distance is in general different than the conventional half-wavelength. In particular, we fix the inter-element distance $d = 0.56\lambda_1$, where λ_1 is the smallest working wavelength. As a consequence, when the RIS is used at the larger λ_2, the array response experiences non-idealities such as mutual coupling, which reduce the main lobe magnitude, and increase both side-lobe level and angular width.

To counteract such issues, we propose a novel optimization framework, namely FABRIS, which aims at finding both the (passive) beamforming configuration and *activation profile* at the RIS to maximize the SLNR at the intended user. Indeed, our novel RIS unit cell design possesses the ability to turn-off antenna elements by using a matched load and thus restoring a higher inter-element spacing, which in turn reduces the mutual coupling across the array.

We consider the wireless network depicted in Figure 3-7, wherein a number of non-intended users are placed in a circular area of radius r around the target user.

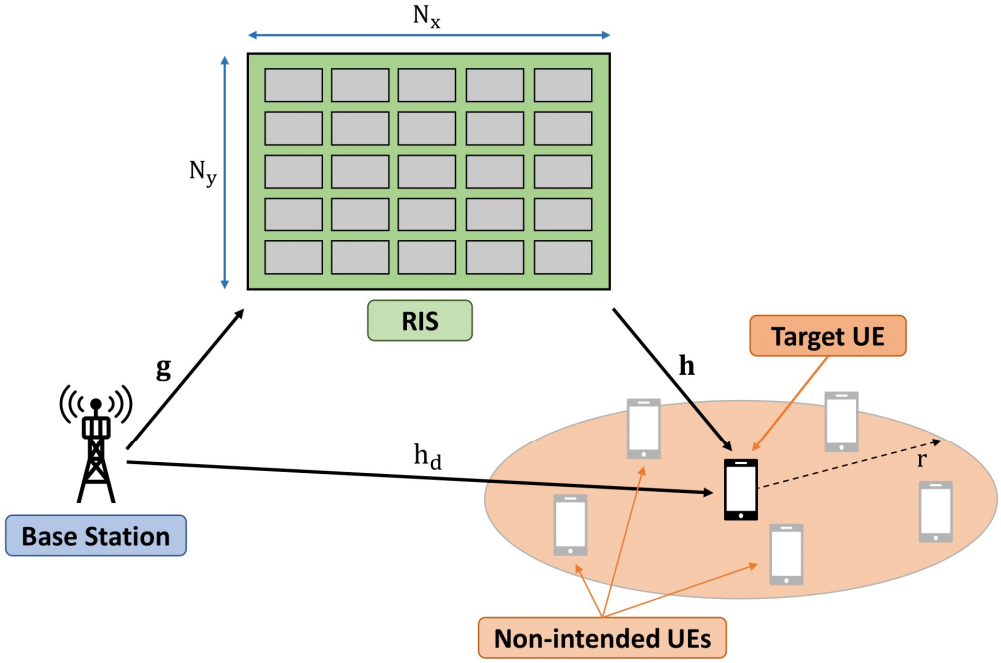

Figure 3-7: Considered system model for multi-frequency RIS design

Methodology

The considered optimization problem is formalized as follows

$$\begin{aligned} \max_{\boldsymbol{\Phi},\boldsymbol{\alpha}} \quad & \mathrm{SLNR}(\boldsymbol{\Phi},\boldsymbol{\alpha},\lambda) \\ s.t. \quad & \alpha_i \in \{0,1\}; \\ & [\boldsymbol{\Phi}]_{i,i} \leq 1, \qquad [\boldsymbol{\Phi}]_{i,j} = 0 \end{aligned}$$

where $\boldsymbol{\Phi}$ represents the RIS phase shifts and $\boldsymbol{\alpha}$ is the (binary) vector of unit cell activations for the specific working wavelength λ.

Such non-convex problem is solved by decoupling the optimization of the phase shifts and activation profile. The former is defined as MRT, while the latter is found by SDR and subsequent rank-1 approximation via Gaussian randomization.

Results and outcomes

In Figure 3-8 we show the CDF of the SNLR in the target area obtained with the proposed FABRIS approach and with a naïve approach with no concern for mutual coupling. The results are shown for $N = 100$ RIS elements and for different values of the target area radius on the left-hand side, and for $r = 10$ m and different values of N on the right-hand side. We notice that FABRIS effectively reduces leakage to neighboring users by suitably optimizing the RIS activation profile as to mitigate the effects of mutual coupling, without excessively compromising beamforming gain, thus obtaining a sweet spot in the trade-off between the two. This effect is

more evident for smaller values of r, since the non-intended users may be very close to the target user and thus experience strong leakage.

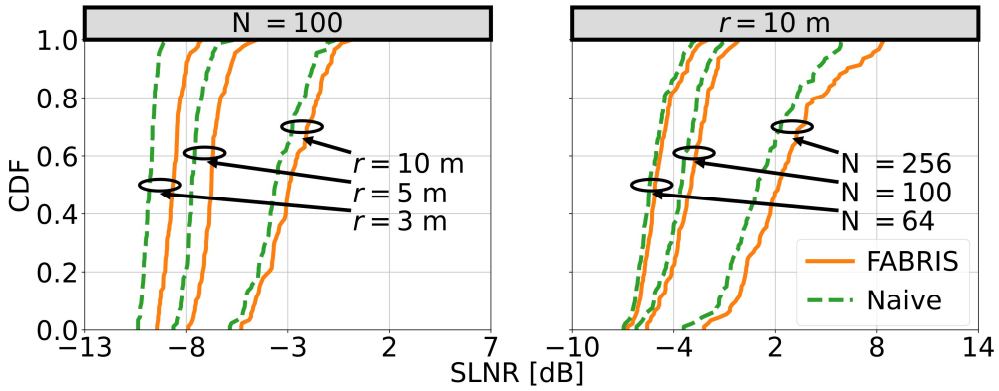

Figure 3-8: CDF of the SLNR obtained with FABRIS and with a conventional Naive approach for different values of target area radius (left-hand side) and RIS elements (right-hand side).

Perspective and relation to other WP4 contributions

This contribution is a first attempt at designing a multi-frequency RIS, which may be used by a single operator to serve users scheduled at different frequency bands, or by multiple operators. In both cases FABRIS allows to effectively share the same hardware without having to change it or opt for redundant deployments.

It may be incorporated into other WP4 contributions as to define the appropriate network architecture and design the associated control channel to support for such kind of solution.

3.5.4 Contribution #A-3: A Self-Configuring RIS Solution Towards 6G

Motivation and context

We propose the novel concept of self-configuring RIS, which can autonomously reconfigure without relying on a dedicated control channel between the RIS controller and the network, to enhance the communication performance in a multi user scenario . Due to the lack of control channel, the configuration of the RIS is based only on local CSI obtained through a channel estimation model lato-sensu at the RIS, which provides enough information on the BS-RIS and the RIS-UEs channels to enable the self-configuration of the RIS. In particular, the RIS self-configures to provide additional, potentially high-gain, reflected paths between the BS and the UEs, thus improving the overall end-to-end channel conditions. The additional high gain reflected paths offered by the RIS can be sensed by the communicating devices, i.e., BS and UEs, via standard channel sounding techniques, and can be exploited for enhancing communication performances.

In order to get sensing capabilities at the RIS, we consider a RIS hardware architecture comprising an array of hybrid meta-atoms able to simultaneously reflect and absorb (i.e., sense) incident signals. Each element of the RIS is coupled with a sampling waveguide that propagates the absorbed portion of the signal downstream an RF circuit comprised by a set of RF combiners that sum the signals sensed by each metasurface element and feed a power detector.

Methodology

We address the RIS self-configuration problem aiming at finding the RIS configuration that provides the better channel enhancement while targeting the achievable sum-rate maximization

problem. With the availability of a control channel, the sum-rate maximization problem can be conveniently solved via alternate optimization of the BS precoder and RIS configuration [MDS21], however it cannot be solved locally at the RIS due to the lack of CSI of the direct link between the BS and each UE. Therefore, we develop a feasible and effective solution that consists in the optimization of the RIS configuration aiming at the enhancement of the end-to-end RIS-assisted channel gain of each user. Upon completion of this optimization, the BS can optimize the precoding matrix according to the equivalent RIS-assisted link.

To build our solution, we firstly find the RIS configuration that maximizes the gain of the reflected paths between BS and UEs. Secondly, we derive a closed form expression that links the aforementioned reflection configuration with the RIS array response vectors maximizing the absorbed power from the BS and the UEs. Finally, we demonstrate that the maximization of the sensed power depends only on the RIS array response vectors pointing towards the AoA in the BS and UE directions, Thus, it is independent of the BS precoding vector and can be fully performed locally at the RIS.

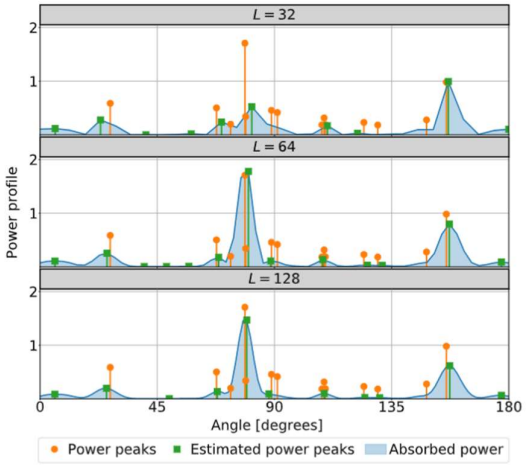

Figure 3-9 Example of power profile and corresponding estimated AoA for different codebook sizes L in a multi UE scenario

We propose a codebook-based approach for estimating the necessary AoA and then computing the RIS configuration locally at the RIS, namely MARISA. Our approach foresees two possible operation modes: probing and communication. In the probing mode, the RIS iteratively sweeps across all the codewords (i.e., beam formers) in the codebook to scan the 3D space in different directions and detect (i.e., sense) network devices. The set of power measurements collected builds a power profile allowing the RIS to estimate locally the AoAs of the transmitting devices, as depicted in Figure 3-9. Upon completion of the probing phase, the RIS enters into the communication phase, which is aimed to assist the reliable transmission of data between the BS and the active UEs. In this phase, the end-to-end RIS optimal configuration is computed from the obtained AoAs and then projected onto the feasible set of discrete phase shifts according to the RIS hardware capabilities.

Results and outcomes

To assess the performance of the self-configuring RIS, and verify its feasibility, we consider a squared service area wherein a single BS and a single RIS are located in the midpoint of adjacent edges. We consider uniform UEs distribution and compare the performances of our self-configuration scheme against the centralised approach proposed in [MDS21], which jointly optimises the RIS configuration and BS precoder with perfect CSI availability.

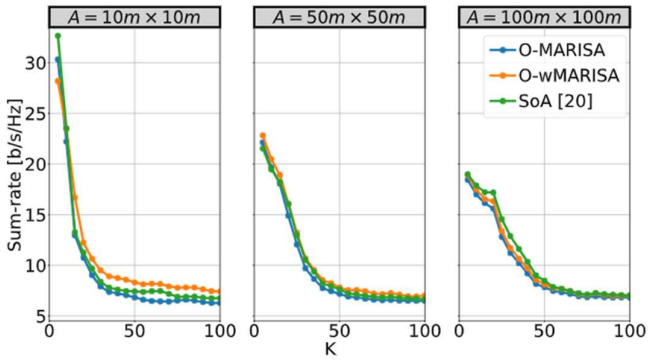

Figure 3-10 Average sum-rate in a multi-UE scenario obtained with RIS self-configuration strategy against centralised joint RIS and BS pre-coder optimisation.

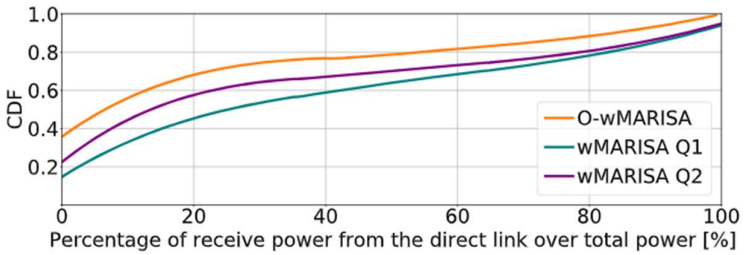

Figure 3-11 Cumulative distribution function of the fraction of the received power at each UE over the direct path with respect to the total received power after precoder optimisation at the BS.

Figure 3-10 provides the performance in terms of the sum-rate obtained with the proposed self-configuration scheme against the centralised approach with different number of users dropped in the service area and with different service area size, while Figure 3-11 depicts the fraction of power transmitted over the additional reflected path. The results demonstrate that the proposed approach provides near-optimal sum rate performances when compared to fully CSI-aware benchmark schemes that rely on a dedicated control channel.

Perspective and relation to other WP4 contributions

The contribution shows the feasibility of RIS self-configuration strategies without involving a centralized controller and provides an effective RIS optimization strategy based on local CSI at the RIS. The contribution is providing an agile deployment strategy which is in line with the work package objective.

3.5.5 Contribution #A-4: Statistical mechanics methods for RIS optimization: Ising Hamiltonian and Quantum Annealing

Motivation and context

We consider the RIS in Figure 3-12: RIS geometry and micropixel structure. **Erreur ! Source du renvoi introuvable.**and use a discrete model to describe the EM scattered field both in free-space and in presence of obstacles. We focus on DL scenario and assume that the base station is in LoS with the RIS, but some blockage occurs with the UEs. We further assume that all the UEs are static and in LoS with the RIS. Both base station and UEs are in the far-field of the RIS. We present an physics-based model of the RIS and related combinatorial optimization algorithm on quantum annealers to tackle the multi-user optimization of large RISs [GDR21]. In beyond

5G networks, the UEs can also be dynamic and therefore experience fading, as in case of devices such as cars, phones, tables or wearables. The statistical mechanics model adopted in this context is prone to include fading as random wave interaction between unit cells of the RIS.

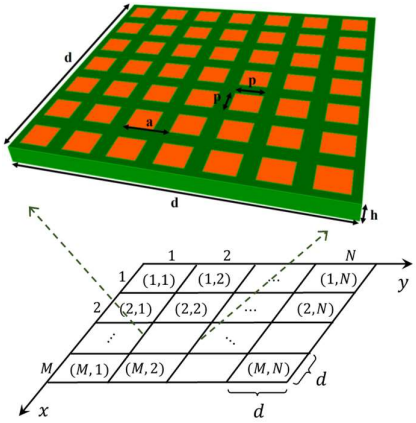

Figure 3-12: RIS geometry and micropixel structure.

Methodology

This contribution describes an isomorphism between the optimization of the RCS of an RIS and the ground state search through an Ising Hamiltonian model. An RIS with multi-level reflection phase $\Phi(m,n)$ codebook is considered for each cell (m,n). An example with RIS binary unit cells mapped onto a two-dimensional spin array lattice $s(m,n)$ is shown in Figure 3-13, spin up and spin down correspond to Dirichlet $(\psi(m,n)=0)$ and Neumann $(\psi(m,n)=\pi)$ boundary conditions respectively, according to the rule

$$s(m,n) = e^{j\Phi(m,n)} = \begin{cases} +1 \\ -1 \end{cases}$$

Both beam-forming and null-forming can be achieved via ground state search of the Ising Hamiltonian of the spin array mapping the RIS. The search has been carried out efficiently via quantum annealing, which proves superior to classical quantum annealers for large RIS dimensions [LRG22]. The technical procedure implementing the Ising Hamiltonian onto a quantum annealer follows three steps [RGL22]:

1. **Biasing step**: Virtual magnetic field applied to prepare particle spins.
2. **Multi-level optimization**: Sub-array division of the spin array, optimization of the individual subarrays and optimization of the array of sub-arrays.
3. **Multi-phase extension**: Definition of complex spins and formation of reflection phase codebook by linear combination of complex-valued spins.

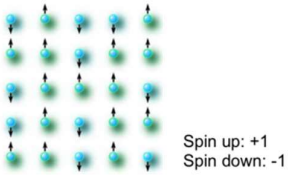

Figure 3-13: Spin array lattice mimicking a binary RIS.

As an example of multi-phase codebook, the macropixel cell dimension p is reported in Table 1-1 for a quadriphase RIS.

p	4.9mm	4.525mm	4.12mm	3.35mm
$\psi(m,n)$	0°	90°	180°	270°

Table 3-2: Phase codebook and associated micro-cell parameters

Results and outcomes

The structure considered in this contribution is the one depicted in Figure 3-12. The whole RIS is formed of 8 x 8 quadriphase macrocells. The operating frequency of the impinging plane wave is set to 8.57 GHz.

1) One-dimensional RIS performance and N^2 law verification. The *RCS* results are reported in Figure 3-14 for an increasing number of RIS unit cells *N*.

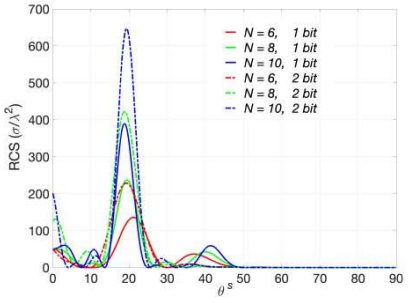

Figure 3-14: One-dimensional RIS performance

2) Joint beam- and null-forming optimization of the RIS. Both the RCs and related RIS mask is reported in Figure 3-15.

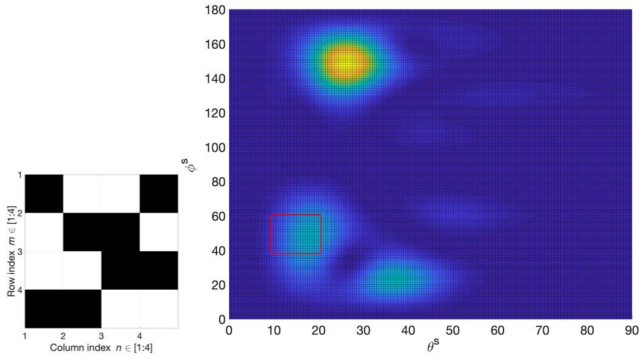

(a)

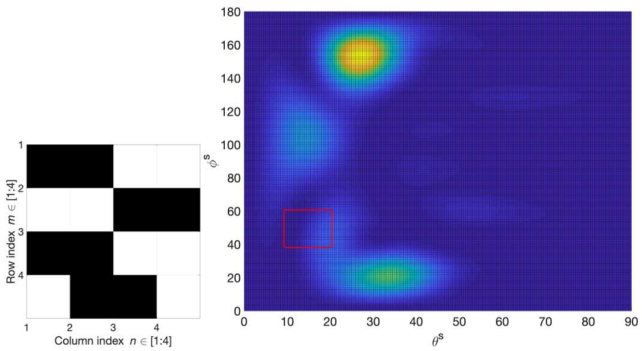

(b)

Figure 3-15: Two-dimensional RIS optimization for: (a) Beamforming; (b) Joint beam- and null-forming within the red square.

3) Comparison between optimization achieved with a physical optics model and full wave simulations for a quadri-phase RIS structure. The RCS of the optimized RIS is reported in Figure 3-16.

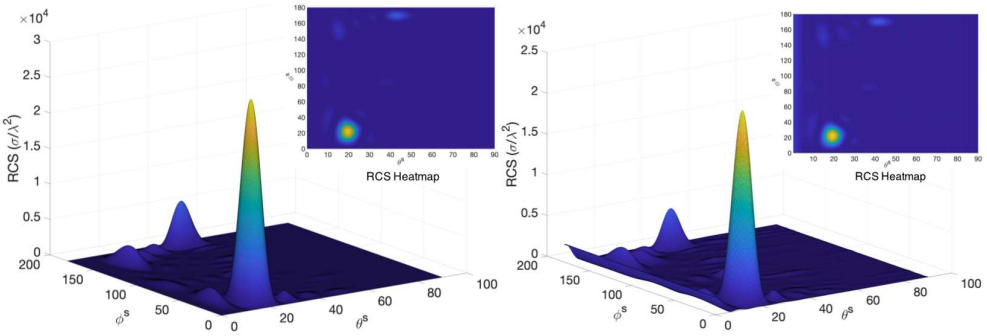

(a) (b)

Figure 3-16: optimized two-dimensional RIS from: (a) Physical Optics model; (b) Full-wave simulations.

Perspective and relation to other WP4 contributions

The contribution provides a physics-based model of the RIS that includes practical constraints. The superior performance achieved by the quantum computation scheme provides a useful tool to tackle the design of large and dense (or multiple) RISs operating in multi-user environments. The approach can be extended to include the presence of object clusters and walls, for which the mathematical structure of the Ising Hamiltonian becomes more involved due to higher order terms, but remains computable via computer architectures of quantum annealers.

3.5.6 Contribution #A-5: Mutual Coupling Aware Sum-Rate Optimization of Reconfigurable Intelligent Surfaces Based on a Mutual Impedance Channel Model

Motivation and context

To evaluate the performance and to optimize RIS-assisted wireless networks, it is necessary to use communication models that account for the electromagnetic characteristics and physical implementation of the RISs. The authors of [GD21] have introduced an electromagnetic consistent model for RIS-aided communications, which resembles a multiple-input multiple-output (MIMO) channel. Departing from [GD21], the authors of [QD21] have introduced an analytical framework and a numerical algorithm that optimize the tunable impedances to maximize the received power. This algorithm introduced is applicable to single antenna transmitters and receivers. Also, a single RIS and a single receiver are considered. In this work, we introduce an algorithm to optimize the sum-rate of an RIS-assisted MIMO interference network that comprises many multi-antenna transmitters, receivers, and RISs. The proposed approach leverages the weighted minimum mean square error (wMMSE) and the iterative block coordinate descent (BCD) algorithms.

Methodology

We consider the MIMO interference channel in Figure 3-17 that comprises N_u transmitter-receiver pairs. Each transmitter and receiver are equipped with M and $L \leq M$ antenna elements, respectively. Each transmit dipole is driven by a voltage generator that models the transmit feed line, and each receive dipole is connected to a load impedance that mimics the receive electric circuit. Differently than Section 2.1, we denote the number of UEs and transmitters as N_u, the number of RISs as K, and the number of RIS elements as P.
The transmission between the N_u transmitter-receiver pairs is assisted by K RISs. Each RIS comprises P nearly passive thin wire dipoles that are independently configurable (by an external controller) through tunable impedances. The indices j, k, and i denote the jth transmitter, kth RIS, and ith receiver, respectively.

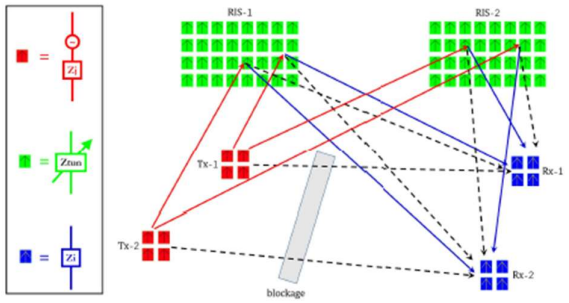

Figure 3-17 Illustration of an RIS-assisted MIMO interference channel ($N_u = 2, M = 4, L = 4, K = 2, P = 32$).

In this work, we consider the case study in which the M-antenna transmitters and L-antenna receivers are in the far-field of each other and in the far-field of the RISs. However, the P thin dipoles that comprise each RIS are arbitrarily close to each other, and the mutual coupling among them is taken into account.

The end-to-end channel matrix from the jth transmitter to the ith receiver can be modeled, in the far-field region, as

$$H_{i,j}(\mathcal{B}) \approx \bar{H}_{i,j} + \sum_{k=1}^{K} \tilde{H}_{i,k,j}(\mathcal{B}) \qquad \in C^{L \times M} \qquad (3.6.1)$$

where $\bar{H}_{i,j}$ accounts for the line-of-sight link and $\tilde{H}_{i,k,j}$ accounts for the (virtual line-of-sight) link re-radiated by the kth RIS. Differently than Section 2.1, we denote the RIS tunable impedances as $\mathcal{B}$. In (3.6.1), we have made explicit the dependence of the re-radiated field with the diagonal matrix $B_k = diag(b_k)$ of tunable impedances of the K RISs. In particular, $\mathcal{B} = \{b_1, b_2, \dots, b_K\}$ is a shorthand for the K vectors b_k to optimize.

By taking into account the concurrent transmissions of the N_u transmitters, the signal at the ith receiver is

$$y_i = H_{i,i}(\mathcal{B})x_i + \sum_{j=1, j\neq i}^{N_u} H_{i,j}(\mathcal{B})x_j + n_i \qquad \in C^{L\times 1} \qquad (3.6.2)$$

where $n_i \in C^{L\times 1}$ denotes the additive white Gaussian noise with distribution $C\mathcal{N}(0, \sigma_i^2 I_L)$. Based on the resulting MIMO interference channel in (3.6.2), the achievable rate of the ith transmitter-receiver pair can be formulated as [A21]

$$R_i(\mathcal{V}, \mathcal{B}) = \log\det(I_L + V_i^H H_{i,i}^H(\mathcal{B})\, \bar{\mathrm{J}}_i^{-1} H_{i,i}(\mathcal{B})\, V_i) \qquad (3.6.3)$$

where $\bar{\mathrm{J}}_i$ is the interference+noise covariance matrix and $\mathcal{V} = \{V_1, \dots, V_{N_u}\}$ collects the N_u precoding matrices.

We aim to optimize the matrices $\mathcal{V}$ and the vectors $\mathcal{B}$ for maximizing the system sum-rate. The sum-rate maximization problem reads

$$\max_{\mathcal{V},\mathcal{B}} R_{tot}(\mathcal{V}, \mathcal{B}) = \max_{\mathcal{V},\mathcal{B}} \sum_{i=1}^{N_u} \alpha_i R_i(\mathcal{V}, \mathcal{B}) \qquad (3.6.4)$$

$$s.t. \quad tr\left(V_i\, V_i^H\right) \le P_i \quad i = 1, \dots, N_u$$

$$\Re\left(b_{k,p}\right) = R_0, \quad k = 1, \dots, K, p = 1, \dots, P$$

$$\Im\left(b_{k,p}\right) \in \mathbb{R}, \quad k = 1, \dots, K, p = 1, \dots, P$$

Where P_i is the power budget of the ith transmitter, $\alpha = [\alpha_1, \dots, \alpha_{N_u}]$ is the set of weights that ensure some fairness among the N_u transmitter receiver pairs and $R_0 \geq 0$ is the resistance modeling the losses of the tunable impedances of the RIS elements.
The problem in (3.6.4) is not convex in the matrices $\mathcal{V}$ and in the vectors $\mathcal{B}$. The proposed approach to tackle it is given in Algorithm 1. At each iteration of Algorithm 1, we solve first (3.6.4) as a function of $\mathcal{V}$ by assuming $\mathcal{B}$ fixed, and then (3.6.4) as a function of $\mathcal{B}$ by assuming $\mathcal{V}$ fixed. Algorithm 1 combines, at each iteration, the solutions of the two sub-problems by using the BCD method.

Algorithm 1: BCD for RIS Optimization

Initialize: RIS impedances $\mathbf{B}_k^{(0)}$; precoding matrices $\mathbf{V}_i^{(0)}$;
small increment $0 \leq \delta \ll 1$; number of iterations $\mathcal{Q}$;
for $q = 1, \dots, \mathcal{Q}$ **do**
  Compute $\mathbf{G}_i^{(q)}$, $\mathbf{W}_i^{(q)}$ and $\mathbf{V}_i^{(q)}$ from Algorithm 2;
  for $k = 1, \dots, K$ **do**
    Compute $\mathbf{M}_k$ and $\mathbf{u}_k$ according to (27);
    Compute δ_k according to (28);
    $\mathbf{B}_k^{(q+1)} \leftarrow \mathbf{B}_k^{(q)} + \Delta_k$;

Algorithm 2: wMMSE for Precoding Optimization

Define: $\mathbf{E}_i(\mathcal{V}, \mathbf{G}_i, \mathcal{B}) = \mathbf{I}_L - 2\Re\left(\mathbf{G}_i^H \mathbf{H}_{i,i}(\mathcal{B})\mathbf{V}_i\right) + \sigma_i^2 \mathbf{G}_i^H \mathbf{G}_i$
$+ \sum_{j=1}^{N_u} \mathbf{G}_i^H \mathbf{H}_{i,j}(\mathcal{B})\mathbf{V}_j \mathbf{V}_j^H \left[\mathbf{H}_{i,j}(\mathcal{B})\right]^H \mathbf{G}_i$;
for $i = 1, \dots, N_u$ **do**
  $\mathbf{J}_i = \sum_{j=1}^{N_u} \mathbf{H}_{i,j}(\mathcal{B})\mathbf{V}_j^{(q)} \left[\mathbf{V}_j^{(q)}\right]^H \left[\mathbf{H}_{i,j}(\mathcal{B})\right]^H + \sigma_i^2 \mathbf{I}_L$;
  $\mathbf{G}_i^{(q+1)} = \mathbf{J}_i^{-1} \mathbf{H}_{i,i}(\mathcal{B})\mathbf{V}_i^{(q)}$;
  $\mathbf{W}_i^{(q+1)} = \left[\mathbf{E}_i\left(\mathcal{V}^{(q)}, \mathbf{G}_i^{(q+1)}, \mathcal{B}\right)\right]^{-1}$;
  $\mathbf{K} = \sum_{j=1}^{N_u} \alpha_j \left[\mathbf{H}_{j,i}(\mathcal{B})\right]^H \mathbf{G}_j^{(q+1)} \left[\mathbf{W}_j^{(q+1)}\right]^H \mathbf{G}_j^{(q+1)} \mathbf{H}_{j,i}(\mathcal{B})$;
  $\mathbf{V}_i^{(q+1)} = \alpha_i (\mathbf{K} + \mu_i \mathbf{I}_M)^{-1} \left[\mathbf{H}_{i,i}(\mathcal{B})\right]^H \mathbf{G}_i^{(q+1)} \mathbf{W}_i^{(q+1)}$;

Results and outcomes

We consider a setup with two transmitter-receiver pairs ($N_u = 2$) located in $t_1 = (5\ 20\ 1)$, $t_2 = (5\ 10\ 1)$, $r_1 = (5\ 5\ 1)$ and $r_2 = (5\ 25\ 1)$ and two RISs ($K = 2$) centered in $(0\ 20\ 2)$ and $(0\ 5\ 2)$. The transmission frequency is $f = 28\ GHz$ and the wavelength is λ. The number of antennas

at the transmitters and receivers is the same, i.e., $L = M$, and their inter-distance is $\lambda/2$. The RIS scattering elements are thin wires with length $l = \lambda/32$ and infinitesimally small radius a. Also, $R_0 = 0.2\,Ohm$. To assess the impact of subwavelength inter-distances while keeping the simulation time reasonably short, we assume that the size of each RIS is fixed to $\lambda \times \lambda$, which may represent a super-cell in a large-size RIS. Thus, the number of scattering elements P and their inter-distances are chosen appropriately, e.g., $P = \{4, 16, 64, 256\}$ for $d = \{1/2, 1/4, 1/8, 1/16\}\lambda$. The noise and transmit powers are $\sigma_i^2 = -120\,dBm$ and $P_i = 20\,dBm$. The transmitters and receivers are assumed to be in non-line-of-sight (the direct links are ignored).

In Figure 3-18, we observe that, if the mutual coupling is taken into account, increasing the number of antennas at the transmitters and receivers enhances the sum-rate, and an RIS with closely spaced scattering elements yields superior performance. In Figure 3-18, two case studies are analyzed: (i) free space propagation (solid lines) and (ii) multipath propagation (dashed lines). The performance trends are similar in both cases. Also, the sum-rate is higher in multipath propagation case, since the multi-antenna transmitters, the multi-antenna receivers, and the RISs exploit the presence of additional propagation paths.

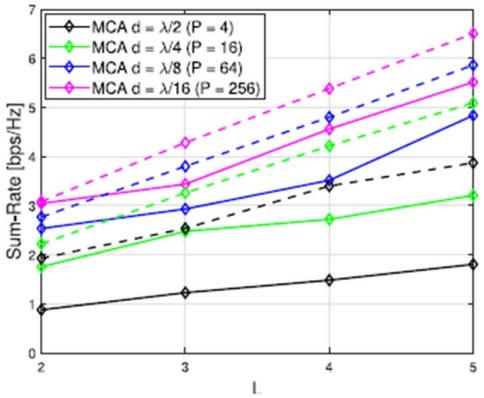

Figure 3-18 Sum-rate vs. L (10000 iterations)

Perspective and relation to other WP4 contributions

We have introduced an optimization algorithm for maximizing the sum-rate of RIS-assisted MIMO interference channels. The proposed approach accounts for the mutual coupling among closely spaced scattering elements. Numerical results have validated the convergence of the proposed approach and the need of accounting for the mutual coupling among the scatterers of the RIS at the design stage.

3.5.7 Contribution #A-6: Degree-of-Freedom estimation from ray tracing

Motivation and context

Ray-tracing methods such as Dynamical Energy Analysis (DEA) performed at UNOT are an important tool for simulating the performance of RISs within complex, multi-reflective environments. The calculations presented in this section are intended to leverage the output of such simulations to provide more granular information on the strengths and numbers of available communication channels, which provide input to the metrics such as Spectral Efficiency defined in Section 2.5, enabling us to evaluate their dependence on and sensitivity to the surrounding geometry and physics (including RISs).

Methodology

The input for the calculations developed here is a density of rays $\rho(s,p)$ in which s and p respectively represent the position and direction of a ray as it hits a boundary. Such densities are the direct output of the DEA method, for example. These densities can be directly related to correlation matrices of receiving and transmitting antennae, from which communication rates and channels are determined, using the Wigner correspondence [GCT15]. This correspondence therefore allows us to leverage DEA simulations into direct, quantitative estimates of communication rates between transmitting and receiving patches supporting large MIMO arrays.

Results and outcomes

An important quantitative characteristic of the interaction of transmitting and receiving patches is the quantity $\mathrm{N}_{\max} = k^d A/(2\pi)^d$, in which A is the overlap area in phase space between transmitting and receiving regions and d is the boundary dimension, which estimates the effective maximum number of communication channels for that geometry. Beyond that value, even fully optimized channel strengths drop off rapidly (see Figure 3-19). This is a well-studied problem in the case where the overlap region is a simple rectangle in phase space and quantitative estimates of the transition and fall-off are well known (see, for example, the curves labelled Slepian1 and Slepian2 in Figure 3-19) [S65].

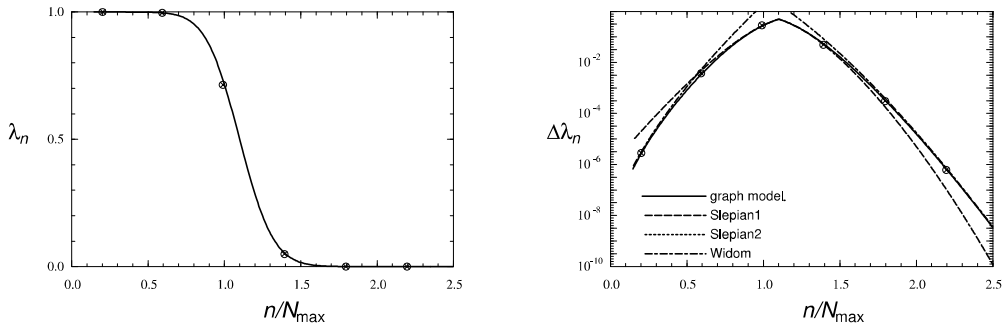

Figure 3-19: DOF estimates from phase-space geometry. On the left are shown the channel strengths for a patch in phase space whose area is such that $N_{max} = 5$ (only even values of n are plotted), which are well described by the newly-developed graph model (continuous curve). On the right we compare the difference between this estimate and the extreme ray limit, where channel strengths drop sharply from 1 to 0 at N_{max}. The graph model gives a better quantitative description over a wider range of n than traditional estimates, which represented by the dashed curves (labelled Slepian1 and Slepian2).

We have developed a new approach to tackle this problem, which leverages on a graph model to study and solve a related differential equation. This graph model achieves the following aims.

- It generalizes the calculation beyond the classically-studied case of a simple rectangular patch in phase space to the case pf skewed patches, which are more characteristic of the problems encountered in multi-reflective environments with large transmitting and receiving areas.
- It applies universally, for all values of the channel label n, whereas classical results are confined to the transition region $n \approx N_{max}$ (see curves labelled Slepian1 in Figure 3-19), to small values of n (see curves labelled Slepian2 in Figure 3-19), or to very large values of n (see curves labelled Widom in Figure 3-19).

These estimates provide a baseline calculation to bound the number degrees of freedom available for a given geometry and physical environment of transmitting and receiving antennas and RISs, but the channel strengths and numbers that are actually realized depend on further fine detail of the ray density $\rho(s,p)$, which is in turn affected by physics such as path loss.

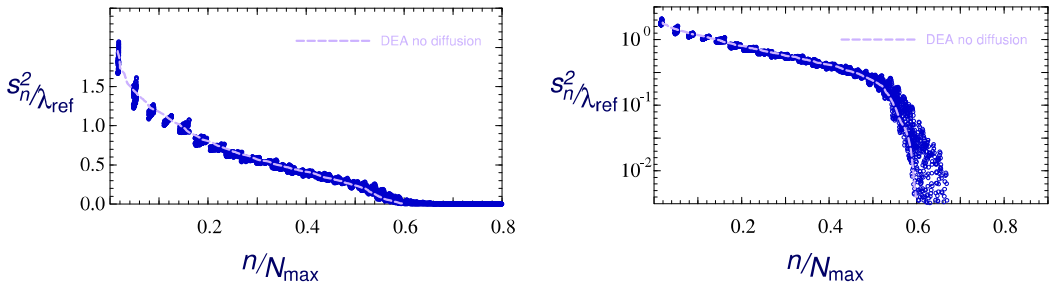

Figure 3-20: Further refinement of DOF estimates can be obtained from the simulated phase-space density $\rho(s,p)$ obtained in these illustrations from DEA simulation of a model two-dimensional cavity. The circles here show individual channel strengths collated from separate simulations performed over a range of frequencies, but with appropriate scaling these are seen to be well described by a prediction obtained from $\rho(s,p)$) (dashed curves). Here the ray density is significant only inside a proper subset of the geometrically-allowed patch in phase space, so the number of effectively available channels is smaller than N_{max}. Furthermore, within the available phase-space area, the density has significant variation, so that there is a corresponding variation of the available channel strengths.

We have been able to leverage DEA simulation into a more refined estimation of channel strengths and numbers using a *Weyl formula* [D78], which approximates a density of eigenvalues λ_n (channel strengths) in terms of the profile of the phase space density $\rho(s,p)$. So far this has been tested against model 2D cavities at relatively low frequencies, where wave effects are important, but as shown by the example in Figure 3-20, is nevertheless capable of providing detailed quantitative predictions.

Perspective and relation to other WP4 contributions

The calculations completed so far have provided an important proof-of-principle of the efficacy of ray-tracing approaches such as DEA in providing detailed, granular approximation of the available communication rates between given transmitting and receiving LISs, but it must be acknowledged that significant further development will be necessary. In particular, these methods have so far been tested only on lower-dimensional and simplified geometries and must in the future be lifted to more realistic (2D or 3D) geometries. In addition, the explicit incorporation of RISs is yet to be performed, although this is a challenge mostly for the DEA method itself and it does not constitute a significant barrier to the DoF estimates under consideration in this part. Once fully developed, such DoF quantification will provide useful input into the evaluation of metrics and KPIs set out in Section 2, for example.

3.5.8 Contribution #A-7: Frequency-Mixing RIS for Nonlinear Wireless Propagation

Motivation and context

We propose a novel concept of RIS which acts as a frequency mixer with a given frequency, named Frequency-Mixing RIS (FMx-RIS), shown in Figure 3-2121. The architecture relies on sinusoidal adjustment of the reflection amplitude with a certain frequency, uniquely associated

with a given surface, which makes the wireless propagation environment non-linear introducing new frequencies. This feature simplifies the channel estimation (CE) in RIS-aided systems since the channels from each RIS can be estimated in parallel in the frequency domain, potentially leading to a large decrease in the estimation overhead. We examine the concept from a communication-theoretic viewpoint and elaborate the unique way to identify the channel from different propagation paths.

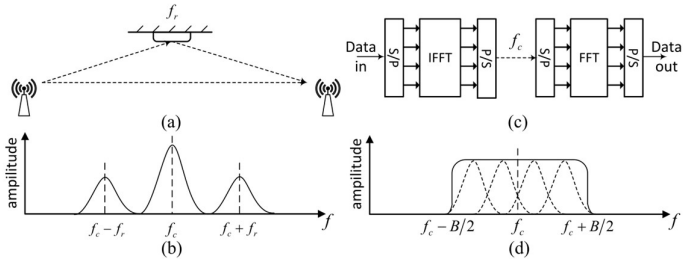

Figure 3-21 A simple example of an FMx-IRS-aided system is shown in (a), where a single-antenna transmitter communicates with a single-antenna receiver aided by an FRM operating on frequency f_r; (b) shows the corresponding frequency response of the received signal; (c) give an example of a wide-band system with carrier at f_c and bandwidth B, and (d) shows the corresponding frequency response. [YWD21]

Methodology

We start with the two-path channel model to describe the details of the operation and introduce the basic principles behind FMx-RIS, where the incident signal is multiplexed to other two frequency bands that uniquely associates with the operating frequency at RIS. Then we consider the infinite-path channel model to develop guidelines for choosing operating frequency at the surface to minimize, potentially remove the correlations between the reflective channels from RIS. In addition, we investigate the CE in the uplink direction and verify the feasibility of the pilot-based CE scheme for both two-path model and multipath model without requiring extra pilot overhead. Finally, we derive the upper bound of the achievable rate that can perfectly predict the system performance. The interested reader can refer to [YDW21] for all the details on the system model, problem formulation, and algorithmic solutions.

Results and outcomes

Figure 3-2222 compares the channel gain of the classical two-path model and the two-path model in which one of the paths goes through an FMx-RIS. In contrast with classical two-path model, FMx-RIS decouples the two paths in frequency and avoids this superposition, which stabilizes the channel gain of the received signal as a function of distance. Figure 3-2323 exhibits the normalized MSE (NMSE) of channel estimation under different propagation environment. The estimation performance of the direct path outperforms that of the reflected path at low-SNR due to the fact that frequency-mixing operation splits the power, and the effect of noise on channel estimation at low SNRs is much higher. Figure 3-2324(a) illustrates the condition number of effective channel to show the channel diversity gain which indicates the optimal FMx-RIS operating frequency ($i \in \mathrm{N}^+$) that maximizes the diversity gain. Figure 3-2424(b) shows that the upper bound converges to the real achievable rate really tight, and offers a considerable gain compared with conventional MIMO due to the extra contribution from the reflective paths.

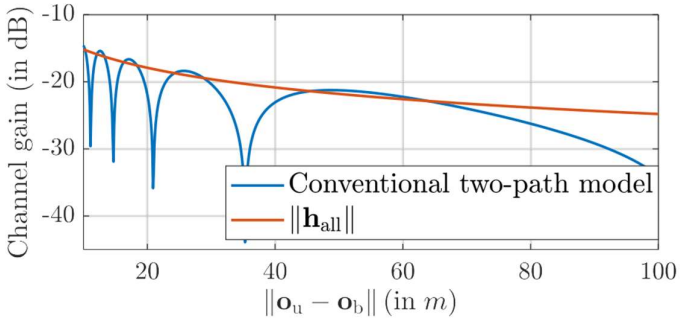

Figure 3-22 Pathloss v.s. distance between user and BS under two-path model [YDW21]

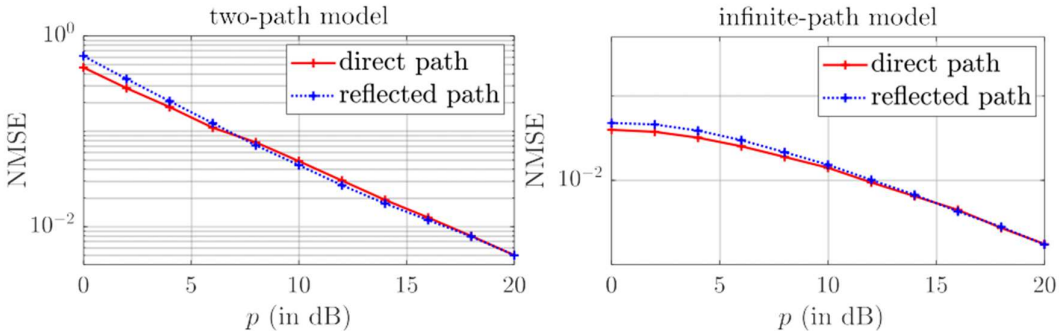

Figure 3-23 Channel NMSE v.s. the transmit power for different channel model [YDW21]

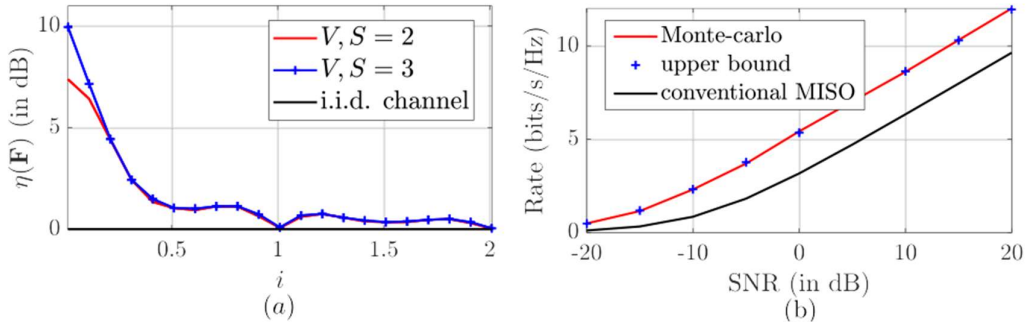

Figure 3-24 Impact of correlation among reflected paths under infinite-path model, where (a) shows the conditioning number w.r.t i being normalized frequency shift; (b) compares the capacity upper bounds with real capacity [YDW21]

Perspective and relation to other WP4 contributions

The use of the RIS as frequency mixer may be a revolutionary approach able to reduce the complexity of the channel estimation phase at the cost of increasing the occupied bandwidth. This can be extremely useful for communication purpose, being the CSI estimation a fundamental step for the communication process and at the same time very resource consuming when performed by entities employing a large number of antennas.

4 Design of Multi-User Techniques for RISE Communications

The design of RIS-aided communication techniques for multi-user environments should take into consideration the different aspects of access, channel estimation, communication parameters optimization and data transmission already considered for classical wireless systems. Differently from 5G standard communications, RIS populated networks need particular attention on the impact the phase shift profile can have in the various operations. The configuration of the RIS can be used to increase the performances of a single data transmission, but can also be used to perform opportunistic variation of the environment improving the performance of various operations.

In this section, we present consideration on the design of the various phases of RIS-aided wireless communications.

4.1 RIS-aided access procedures

The access procedure regards the admission of one or more users to the network. The approach used in the 5G networks make use of DL synchronization signals transmitted by the BS. The users listen to the incoming signal trying to decode the information within, and then try to connect to the BS using synchronization and access messages. In case of MIMO BS, the DL synchronization signals are transmitted multiple times, while the beamforming of the BS sweeps to a certain number of beamformer vectors enabling it to cover the area of interest.

As already presented in Deliverable 4.1, a similar procedure can be employed by the RIS-aided network, in which the RIS may sweep through a set of possible configurations [CSL22]. Using a DL transmission phase, we let the UEs learn which configuration provides a sustainable SNR. Exploiting this information, each UEs can send pilot signals during the access (UL) phase in the attempt to access the network. Here, we stress the necessity of a careful design of 1) the set of configurations available at the RIS and 2) the estimation techniques at the UE.

On the configuration design, we need to specify a codebook of fixed configuration that can be selected in sequence by the RIS controller when the access procedure is triggered. Generally, the codebook should contain enough configurations to cover at least the whole area of interest. In this way, each user in the scenario can receive the synchronization signal and try to access the network.

From the UE perspective, a sequence of signals are received during the DL transmission phase. The UE can then apply signal processing techniques to recover the function that characterizes the channel gain over configurations. Depending on the estimation technique, the number of the configuration of the access codebook might be increased to provide good estimation performance, needed for selecting the slot of the access phase providing the best gain.

We remark that sweeping through configuration generates spatial diversity and may reduce the number of collisions. However, a large number of configurations increase the time for the configuration estimation phase, reducing the available throughput. Hence, the design of codebook and estimation techniques must take into account this trade-off.

4.2 CSI estimation in multi-user RIS networks

The estimation of channel state information (CSI) may be the bottleneck in the design of communication techniques for RIS-aided systems. The presence of the RIS constrains the system to estimate multiple channels simultaneously, whose dimension increases with the number of elements of the RIS itself. This is particularly challenging considering that a high number of elements is desirable for increasing the gain provided by the RIS. We remark that

this is even more important for nearly-passive and quasi-active RISs that are not equipped with active transmitting RF chains and are unable to boost the received signal (see Table 1 of Deliverable 4.1 for the formal definition of this kind of hardware). Therefore, the need for fast and accurate CSI estimation techniques is of fundamental importance.

Studying the statistics of the considered channel, we can assume that the BS-RIS channel will change slowly with respect to the RIS-UE channel. Exploiting this feature, a solution based on parallel decomposition and bilinear estimation of the channel has proven to reach good performance with very fast convergence, being able to track time varying channels [YAK22]. However, this method is only suitable when the direct link between BS and UE is blocked and should be modified to also include the direct path.

4.3 Optimization of the RIS configuration

While the general problem of optimizing the beamforming for both BS and RIS has been described in Section 3.1, here we focus on the consideration for providing optimal configurations under more realistic scenarios.

As already mentioned, the CSI estimation is a complex task for the RIS-aided networks. For this reason, it is favourable to design the configuration profiles exploiting other means. A possibility is to capitalize on the strong LoS component of BS-RIS-UE, focusing the beam impinging the RIS towards a particular direction. Moreover, the phase shift profile can be further optimized to scatter signals in different directions at once, enabling multicasting operation at the physical layer.

Also, the optimization design can be made using the information related to the position, reducing the need of CSI estimation. This can be done by means of classical optimization methods or by means of machine learning techniques. An example of the two methods is given in Section 4.4.2 and in Section 4.4.5.

Finally, we remark the importance of learning approaches to optimize the configuration for specific context and objectives. Among them, the reinforcement learning approach is able to react dynamically to the change in the environment, which otherwise leads to reduced performance. Indeed, efficient reinforcement learning algorithms can be designed to jointly exploit the limited CSI data available, the reception of feedback signals on the quality of the communication, and even the hardware non-ideality of the RIS elements. A more detailed description of the capability of such approaches is given in Section 4.4.4.

4.4 Contributions from RISE-6G

The following table lists the relevant contributions from RISE-6G in the design of multi-user techniques for RISE systems

Table 4-1 Contribution of RISE-6G on design of multi-user techniques

Parameter	Scope	Based on	#BS	#RIS	LoS/ NLoS	Continuous/ quantized phase-shift

B-0: Tensor-based Channel Tracking for RIS-Empowered Multi-User MIMO Wireless Systems	Fast CSI estimation	Transmission of pilot, parallel factor decomposition and bilinear estimation	1	1	LoS/ NLos	Continuous
B-1: Sum-Rate Optimization of Reconfigurable Intelligent Surfaces Based on Statistical Position Information	Maximize the throughput	Statistical positioning information	1	1	LoS/ NLos	Continuous
B-2: Beam-sweeping random access protocol for RIS-aided systems	Access of new and intermittently active users	Sweeping trough RIS configurations	1	1	LoS	Continuous
B-3: RIS Orchestration algorithms for online configuration tuning based on Reinforcement Learning	Online configuration optimization	Reinforcement Learning and Multi-Armed Bandit approaches	1	Multi ple	LoS/ NLoS	Quantized
B-4: Supervised learning of optimal phase configuration based on user positions	Phase shift of multiple RIS at once	Deep Neural Network learning approach	1	Multi ple	LoS/N LoS	Quantized
B-5: Reconfiguration of the physical layer for multi beamforming	Multi beamforming toward different receivers	LoS beamforming	1	1	LoS	Continuous

4.4.1 Contribution #B-0: Tensor-based Channel Tracking for RIS-Empowered Multi-User MIMO Wireless Systems

Motivation and context

Channel estimation is of crucial importance for the successful operation of RIS-aided MIMO communication systems. The predominantly passive nature makes the estimation of the channels a quite challenging problem. The problem is even more challenging if the channel is modelled in a time-varying manner to consider a realistic behaviour. The RIS-BS channel changes much more slowly than RIS-UE channel due the fixed locations of RIS and BS. Both RIS-BS link and RIS-UE channels are modelled as the sum of the possible geometric paths. The RIS phase profile is designed operating as cycles of DFT matrix columns.

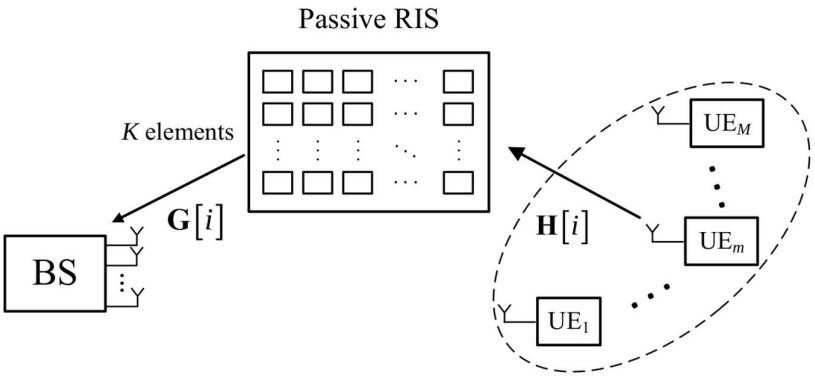

Figure 4-1 System model [YAK22]

Methodology

We aim to estimate the separate channels efficiently and accurately for a scenario comprehending a MIMO BS, a single RIS of K elements and M users, as depicted in Figure 4-1. We first design the transmission protocol where UEs send the pilot sequences multiple times in order to collect sufficient observations for separating cascaded channels. Then, relying on an adaptive Parallel Factor (PARAFAC) decomposition scheme for the received signal at the BS, the initial estimates of RIS-BS and RIS-UE channels are estimated employing the Bilinear alternative least square (BALS). To reduce the complexity, we adopt recursive LS (RLS) to track the variation of the channel leveraging the relatively stationary of RIS-BS channel. This two-step procedure will henceforth be referred to as BALS-RLS. Finally, the sparse nature of the incurred channels is exploited with the aid of a Generalized approximate message passing (GAMP) algorithm.

The interested reader can refer to [YAK22] for all the details on the system model, problem formulation, and algorithmic solutions.

Results and outcomes

Figure 4-2 shows the NMSE performance of the RLS and BALS-RLS as a function of the time slot, considering various RIS sizes K. The RIS-BS channel changed every 100 slots. It can be observed that the proposed BALS-RLS algorithm converges within few time slots in all plotted use cases. Figure 4-3 compares the computational costs of the three considered CE algorithms as functions of the parameter K, and demonstrates the extreme low complexity of BALS-RIS. Figure 4-4 illustrates the channel recovery performance of the proposed GAMP-based algorithm. We observed that a relatively stable CE accuracy is obtained by GAMP with only half of the pilot overhead required for conventional method.

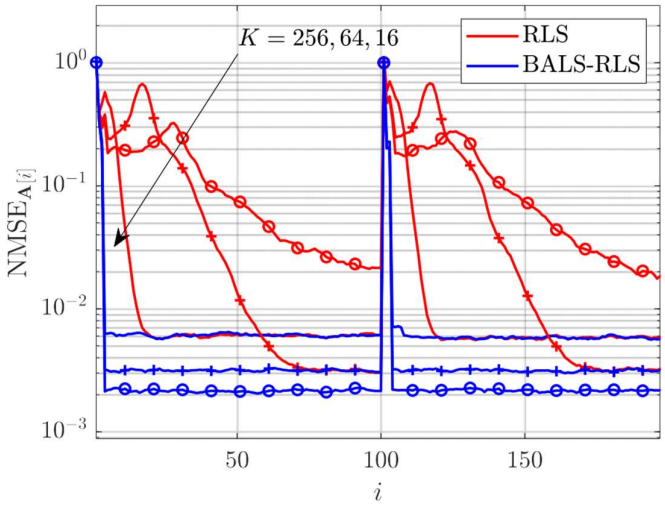

Figure 4-2 NMSE of CE with the RLS and BALS-RLS algorithms versus the discrete time evolution [YAK22]

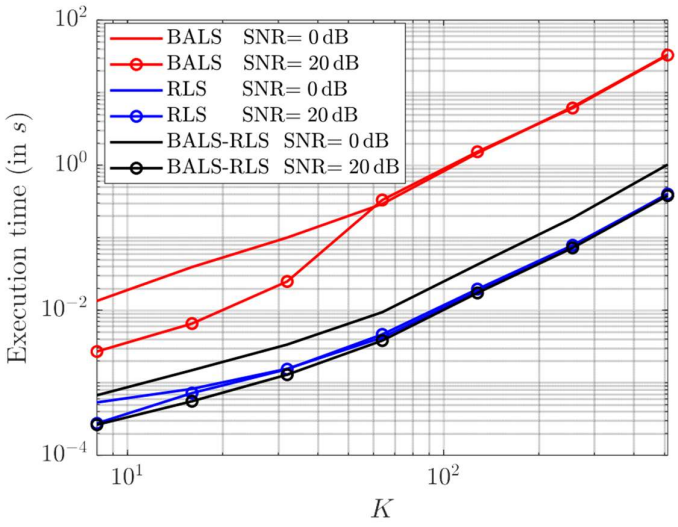

Figure 4-3 Execution time of the BALS-, RLS-, and BALS-RLS-based CE algorithms verse RIS size [YAK22]

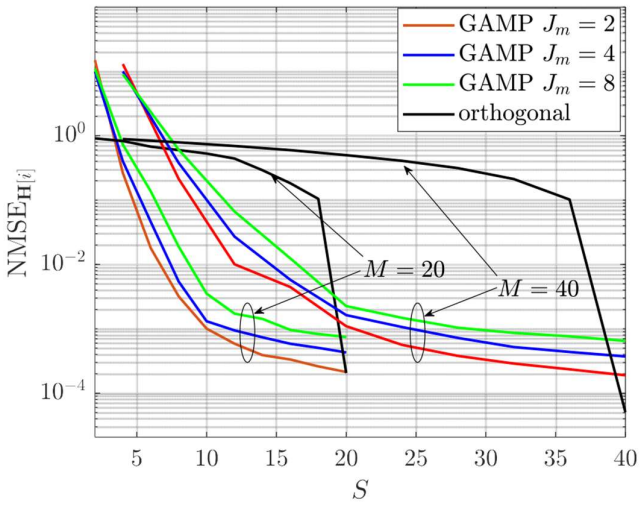

Figure 4-4 NMSE of CE considering GAMP and orthogonal pilots for different pilot sequence lengths [YAK22]

Perspective and relation to other WP4 contributions

Channel estimation is a fundamental task for RIS-aided communication. The proposed channel estimation procedure is able to deal with time-varying channel, providing a procedure to efficiently track the variation of the channel over time with little overhead in terms of slot used for the estimation.

4.4.2 Contribution #B-1: Sum-Rate Optimization of Reconfigurable Intelligent Surfaces Based on Statistical Position Information

Motivation and context

Most research works [YYH20], [H19] and [WZ19] focused on optimizing the performance of RIS-assisted systems are based on the perfect knowledge of the CSI for all the available channels, as well as on the availability of appropriate feedback mechanisms to configure the operation of the RISs based on the acquired CSI. In spite of the relatively large number of research contributions available to date, the channel estimation in RIS-aided systems is still an open issue that is characterized by three major challenges: (i) the long training time, especially in multi-user MIMO (MU-MIMO) systems, which may not be tolerable in dynamic scenarios; (ii) the real-time reconfiguration of the reflection functionality of the RIS through a dedicated control channel with the base station (BS); and (iii) the need of ad hoc channel estimation and signaling protocols that make the deployment of RISs non-transparent to existing communication protocols. To tackle these open research issues, some authors have recently started researching on RIS-aided systems that do not necessarily rely upon the perfect knowledge of the CSI, e.g., [NKC20], [Z20] and [YXN21].

In this contribution, we consider a multi-RIS MU-MIMO system, and we optimize the reconfigurable elements of the RISs and the beamforming vectors at the BS and UEs to maximize the system sum-rate. The main novelty of the proposed approach lies in not requiring either instantaneous CSI or second-order channel statistics for optimizing the RISs, thus relaxing the need for their (real time) configuration. In fact, the proposed approach relies only on the a priori statistical knowledge of UEs locations. To this end, a two-phase optimization process is introduced, which encompasses an offline phase (long-term and sporadic) and an online (short-term and more frequent) phase. During the offline phase, the RISs are optimized. During the online phase, the communication between the BS and the UEs is optimized without interacting with the RISs.

Methodology

We consider the downlink of a wireless system in Figure 4-5 in which one BS equipped with M antennas serves N_u UEs that have L antennas each. In this network scenario, K RISs are deployed in some predefined locations for assisting the communication between the BS and the UEs. Each RIS comprises P nearly passive reconfigurable scattering elements.

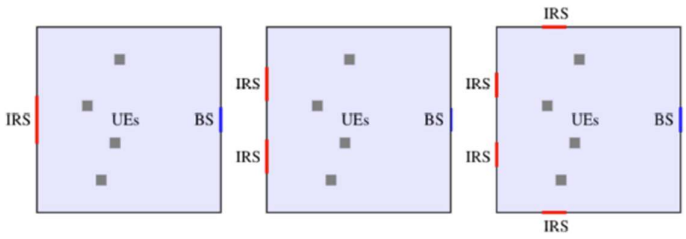

Figure 4-5 Layout of the considered indoor scenario (aerial view) for $N_u = 4$ and $K = 1, 2, 4$

The signal received at the ith UE in the presence of N_u concurrent transmitted streams and K RISs is

$$y_i = H_i(\mathbf{\Phi})x_i + H_i(\mathbf{\Phi})\sum_{j=1}^{N_u} x_j + n_i \qquad \in C^{L\times 1} \qquad (4.4.1)$$

where $H_i(\mathbf{\Phi})$ is the total channel between the BS and the ith UE, $\mathbf{\Phi} = \{\varphi_1, \dots, \varphi_K\}$ is the set of vectors containing the reflection coefficients of the K RISs (analog beamforming vectors), $n_i \in C^{L\times 1}$ is the additive white Gaussian noise with distribution $C\mathcal{N}(0, \sigma_i^2 I_L)$ and $x_i \in C^{M\times 1}$ is the transmitted vector.

Based on the MIMO interference channel in (4.4.1), the achievable rate (AR) of the ith UE is [SRL11]

$$R_i(\mathcal{V}, \mathbf{\Phi}) = \log\det(I_L + V_i^H H_i^H(\mathbf{\Phi})\,\bar{J}_i^{-1} H_i(\mathbf{\Phi})\,V_i) \qquad (4.4.2)$$

where $\bar{J}_i$ is the interference-plus-noise covariance matrix and $\mathcal{V} = \{V_1, \dots, V_{N_u}\}$ is the set of precoding matrices of all N_u UEs.

The proposed approach consists of optimizing the digital beamforming vectors of the BS and the UEs during the online phase, as well as the analog beamforming vectors of the RISs during the offline phase.

In the online phase, the sum-rate maximization problem can be formulated as

$$\max_{\mathcal{V}} \sum_{i=1}^{N_u} \alpha_i R_i(\mathcal{V}) \qquad (4.4.3)$$

$$s.t. \quad tr\left(V_i V_i^H\right) \le P_i \quad i = 1, \dots, N_u$$

where P_i is the BS power budget of the ith UE, $\alpha = [\alpha_1, \dots, \alpha_{N_u}]$ is the set of weights that are chosen to guarantee a given degree of fairness among the UEs.

Algorithm 2 Online Sum-Rate Maximization

Initialize:
Input: φ_k, $k = 1, \ldots, K$, from Algorithm 1;
Evaluate $\mathbf{H}_i(\mathbf{\Phi})$ for $i = 1, \ldots, N_u$;
Generate $\mathbf{V}^{(0)}$ hat fulfill the power constraint;
Set an arbitrarily small value ϵ, $q \leftarrow 1$, $\Delta \leftarrow 1$;
while $\Delta > \epsilon$ **do**
  for $i = 1, \ldots, N_u$ **do**
    Compute $\mathbf{G}_i^{(q)}$, $\mathbf{W}_i^{(q)}$ and $\mathbf{V}_i^{(q)}$
  $\Delta \leftarrow \sum_i \|\mathbf{V}_i^{(q+1)} - \mathbf{V}_i^{(q)}\|$;
  $q \leftarrow q + 1$

In the Offline Phase, the optimization problem for computing $\mathbf{\Phi}$ can be formulated as

$$\max_{\mathbf{\Phi}} \int \max_{\mathcal{V}(\omega)} \sum_{i=1}^{N_u} \alpha_i R_i(\mathcal{V}(\omega), \mathbf{\Phi})\, f_{\Omega}(\omega)\, d\omega \qquad (4.4.4)$$

$$s.t. \quad tr\left(V_i(\omega)\, V_i^H(\omega)\right) \leq P_i \quad \forall \omega, i = 1, \ldots, N_u$$

$$tr\left(\varphi_k\, \varphi_k^H\right) \leq P \quad k = 1, \ldots, K$$

where $f_{\Omega}(\omega)$ is the joint probability density function of Ω, $\Omega = \{\mathcal{R}, \mathcal{T}\}$ is the set whose realizations are given by the random variables ω, $\mathcal{T}$ is the set of random variables given by the multipath components $\tau_{m,n}$ and $\mathcal{R}$ is the set of random variables given by the locations of all UE's antennas.

Algorithm 1 Offline Sum-Rate Maximization

Initialize:
Generate $\mathbf{V}^{(0)}$ and $\varphi_k^{(1)}$, $k = 1, \ldots, K$, that fulfill the power constraint;
Set an arbitrarily small value ϵ, $q \leftarrow 1$, $\Delta \leftarrow 1$;
Generate the Monte Carlo samples ω_n, $\forall n = 1, 2, \ldots, N_s$, from $f_{\Omega}(\omega)$
while $\Delta > \epsilon$ **do**
  for $n = 1, \ldots, N_s$ **do**
    for $i = 1, \ldots, N_u$ **do**
      Compute $\mathbf{G}_i^{(q)}(\omega_n)$, $\mathbf{W}_i^{(q)}(\omega_n)$ and $\mathbf{V}_i^{(q)}(\omega_n)$
  for $k = 1, \ldots, K$ **do**
    for $n = 1, \ldots, N_s$ **do**
      $\bar{\mathbf{M}}_k^{(q)}(\omega_n) \leftarrow 0$
      $\bar{\mathbf{u}}_k^{(q)}(\omega_n) \leftarrow 0$
      Compute $\mathbf{M}_k^{(q)}(\omega_n)$ and $\mathbf{u}_k^{(q)}(\omega_n)$
      $\bar{\mathbf{M}}_k^{(q)} \leftarrow \bar{\mathbf{M}}_k^{(q)} + \mathbf{M}_k^{(q)}(\omega_n)$;
      $\bar{\mathbf{u}}_k^{(q)} \leftarrow \bar{\mathbf{u}}_k^{(q)} + \mathbf{u}_k^{(q)}(\omega_n)$;
    Compute $\varphi_k^{(q+1)}$
  $\Delta \leftarrow \|\varphi^{(q+1)} - \varphi^{(q)}\|$;
  $q \leftarrow q + 1$

A two-phase optimization process was introduced, which encompasses an offline phase (long-term and sporadic) and an online (short-term and more frequent) phase. During the offline phase, the RISs are optimized. During the online phase, the communication between the BS and the UEs is optimized without interacting with the RISs. The main advantage of the proposed approach is that the information needed for RISs optimization can be either known a priori (e.g., one may know that some UEs are confined within a certain area) or can be learned occasionally during the operation of the system by leveraging, for instance, a localization infrastructure.

As for the online phase, we introduce a generalized version of the WMMSE algorithm for application to MU-MIMO systems, shown in Algorithm 2. As for the offline phase, owing to the more involved expression of the per-user rate of MIMO systems with respect to MISO systems, we further generalize the WMMSE method for optimizing the analog beamforming vectors of the RISs, as shown in Algorithm 1.

Results and outcomes

We consider an indoor environment with dimensions $30\,m \times 30\,m$ along the x-axis and y-axis, respectively. The UEs are equipped with $L = 4$ antennas and are deployed randomly on the left-half of the room, i.e., in an area of $15\,m \times 30\,m$, at a height of $1\,m$. The BS is equipped with $M = 16$ antennas and is placed on the opposite side of the room at the position $(15, 30)\,m$ and at a height of $2\,m$. The 16 antennas of the BS are arranged on the $y-z$ plane with 8 antennas along the y-axis and 2 antennas along the z-axis, while the 4 antennas of the UEs are assumed to be randomly oriented. The antenna-element gains at the BS and at the UE are equal to $3\,dB$. The noise and maximum power budget are $\sigma_i^2 = -97\,dBm$ and $P_i = 0\,dBm$. The RISs are placed on the walls that surround the UEs. Each comprising $P = 50$ scattering elements with inter-distance $\lambda/2$ where carrier frequency $= 28\,GHz$.

To evaluate the performance of the proposed offline optimization approach for RISs that relies only upon the probability distribution of the UEs' locations and upon a mismatched probability distribution of the multipath channels, we compare the proposed approach against two benchmark schemes typically considered in the literature: (i) an ideal CSI scheme denoted by I-CSI, in which the RISs are optimized based on the perfect knowledge of the channel matrices, and (ii) a scheme based on statistical CSI, denoted by S-CSI, in which the RISs are optimized based on second-order statistics, e.g., based on the knowledge of the channel covariance matrices as in [Z20]. The numerical results in Figure 4-6, highlight that the NoCSI setup offers similar performance as the I-CSI and S-CSI setups. The largest performance degradation is obtained, as expected, when each UEs has a single antenna, since it is more difficult to reduce the impact of the interference.

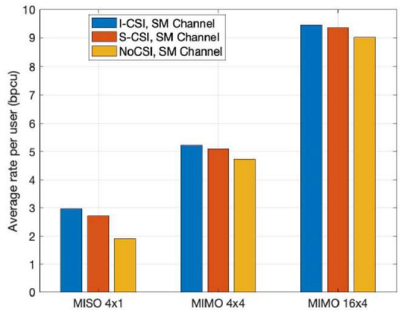

Figure 4-6 Comparison between the I-CSI, S-CSI and NoCSI for three different antenna configurations and for the SM channel model.

Perspective and relation to other WP4 contributions

The main advantage of the proposed approach lies in requiring only the statistical information of the users' position information, thus significantly reducing the overhead associated with the optimization of RIS-assisted wireless systems. The obtained numerical results confirm the validity of the proposed approach. Notably, RIS-assisted wireless systems that are optimized based solely on offline information still provide large performance gains as compared to wireless systems in the absence of RISs.

4.4.3 Contribution #B-2: Beam-sweeping random access protocol for RIS-aided systems

Motivation and context

To extend the coverage of a access point, a network operator can deploy a RIS and offer network access to the UEs affected by blockages.
For this setting, we have proposed a random access protocol in [CSL22]. The aim of this section is to illustrate a random-access protocol based on the spatial dimension given by the RIS.

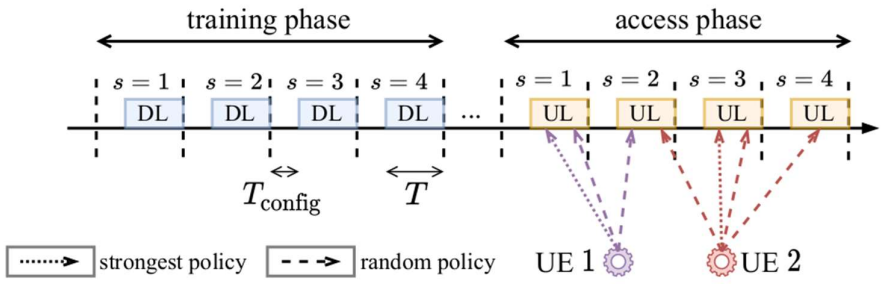

Figure 4-7 Protocol phases for random access of UEs [CSL22]

Methodology

To take into account the different channel conditions experienced by the UEs, the protocol is divided into a DL training phase and an UL access phase, as illustrated in Figure 4-7. In each slot s, a different configuration is set at the RIS. Each configuration refers to a direction of reflection in which the RIS can steer the incoming signal. Such a protocol is based on sweeping through these different configurations in order to cover an area of interest, for both training and access phases.

During the training phase, as this sweeping occurs, the UEs can estimate which of the configurations is most important to them. This configuration estimation phase relies on two main procedures: i) the design of the set of configurations available at the RIS, and ii) the design of an estimator at the UE's side in such a way that they can decide the best configurations later. For the first, we have identified that the design of the set of configurations can be tackled by adopting a signal processing perspective, where each configuration can be seen as a sample of a function that describes the channel gain towards the BS and the UE. Hence, designing a set of configurations is equivalent to designing a sampling strategy. It is possible to obtain bounds on the duration of the configuration estimation phase by using the Nyquist-Shannon theorem and compressed sensing frameworks. Note that, by properly designing the set of configurations, the UEs can recover the function that characterizes the channel gain over configurations. Essentially, the second procedure makes use of recovery methods so that the UEs can know such a function. In this part, we used interpolation methods to reconstruct the signal, and posed compressed sensing problems, such as the basis pursuit denoising. Figure shows an example in which the magnitude of the channel gain is recovered at the UE's side using the LASSO algorithm. After recovering the signal, the UEs are able to choose the best configurations to access the network. The design of the set of configurations used in the access

phase can be performed in a totally separated way to the one of the configuration estimation phase. Essentially, this means that the access phase can optimize to minimize the collision of UEs packets.

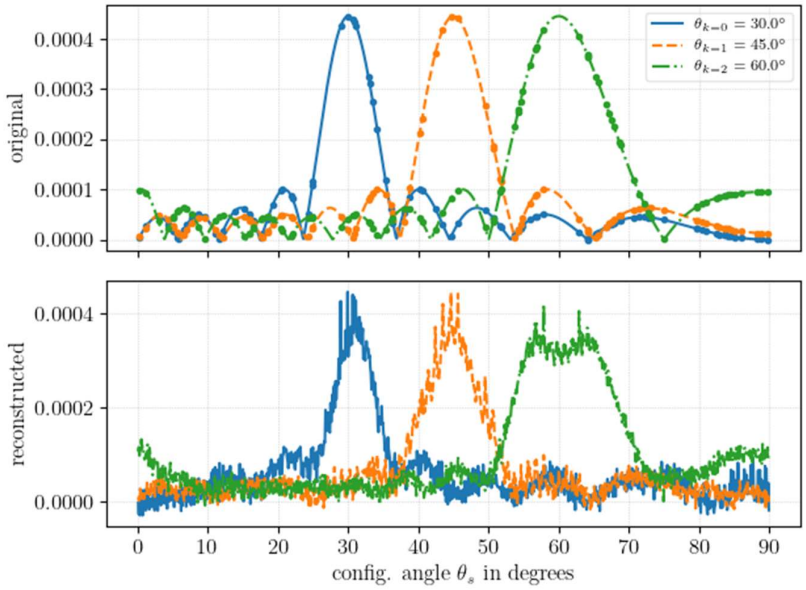

Figure 4-8 Example of reconstruction of the magnitude information of the channel gain along the spatial domain using random sampling and compressed sensing methods.

After the access phase, at the BS, the collision resolution is performed searching for singletons and performing SIC.

The access policies under evaluation are the following:

1. *Strongest-configuration policy (SCP):* each UE chooses the access slot associated to the RIS configuration leading to the best channel quality;
2. *Configuration-aware random policy (CARP):* each UE compute a probability mass function for slot selection with probabilities proportional to the strength of the receiving signal of each configuration. Then, each UE decides the access slots by tossing a biased coin with probability previously computed.

Results and outcomes

As a benchmark, we use the unaware random policy (URP) which does not rely on the training phase; thus, the choice of the access slot is made randomly. Remarkably, RIS-empowered policies outperform random policies when the system gets crowded. The results reveal a very important trade-off for multi-user access, shown in Figure 4-9. On one hand, the use of the RIS to coordinate the access requests from the UEs better resolves collisions, increasing the average number of successful access attempts. On the other hand, the price to pay for RIS help is increased access delay since it depends on the training phase.

Perspective and relation to other WP4 contributions

The proposed random-access procedure can retrieve information on the CSI of the user for every configuration of the RIS involved in the access phase. At the end of the procedure, the BS is informed on which configuration each user prefers for transmission. This information can be used as initialization to RIS profile optimisation algorithms.

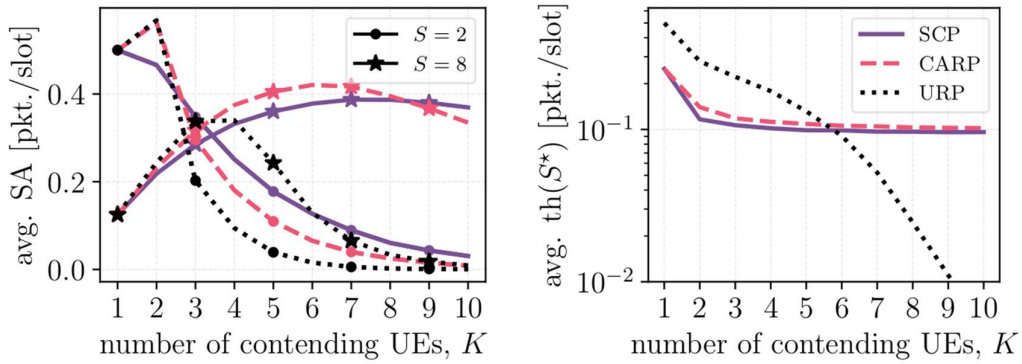

Figure 4-9 Performance of the random-access protocol. Here, S denotes the number of configurations used. The plots show the average number of successful access attempts (left), and the optimal average throughput with respect to S (right). [CSL22]

4.4.4 Contribution #B-3: RIS Orchestration algorithms for online configuration tuning based on Reinforcement Learning

Motivation and context

Traditional RIS deployment methods involve solving an optimisation problem at every channel coherence frame, upon estimating the CSI, in order to find the (near) optimal RIS configuration. While effective, this methodology has the problem of high-computational costs per channel state. Additionally, since each channel state is considered as a standalone sub-problem, the optimisation has to be performed anew, without relying on information observed in the previous state(s). On the other hand, approaches based on machine learning have the advantage of being able to utilise past experience and, after the training period has ended, they are capable of predicting the appropriate configuration with low computational overhead (i.e. in real-time). The main disadvantage associated with this approach is the need for a precompiled data set of channel states and optimal configurations. Apart from the fact that the size of the training data set required for effective learning, cannot be known a priori, such methods are also expected to perform poorly when the distribution of the channel coefficients changes during the deployment phase.

Motivated by the requirements of real-time configuration selection and environmental adaptivity, we tackle the sum-rate maximisation problem using a DRL approach, in which a trainable decision maker continuously observes the CSI and selects the RIS configurations (and precoding matrices) that it expects they will attain the optimal SINR. This neural-network-based agent is trained through a trial-and-error process, during which the observed sum-rates are seen as feedback on the selected configurations and precoders. This methodology has the advantage that it can be either deployed so that its training period continues perpetually (to attain adaptability to environmental changes), or use the pre-trained model without further feedback (in this case, there is no need for measuring and transmitting the received rate values to the decision maker, which entails lower network requirements).

Methodology

We first formulate the joint RIS and precoder beamforming as a RL problem, which entails the following correspondence between the RIS-enabled environment and the RL problem [ASH22]:

- **State:** A vector comprised of all the channel coefficients between the BS and the RISs, the RISs and the UEs, and the BS and the RISs.
- **Action:** A selection among the available RIS configurations and precoding codebook.

- **Reward:** The sum rate of all users (downlink case).
- **Transition:** The agent at time step t observes the state of the environment $\boldsymbol{s}_t$ and selects an action $\boldsymbol{a}_t$. The action is fed back to the environment, which in turns generates the reward r_t and then proceeds to the next time step $t+1$ which involves new channel realisations.
- **Policy:** A mapping between states and actions, i.e. a decision function. The goal of an RL problem is to learn a policy that maximizes the cumulative rewards.

The RL formulation for a single time step is illustrated in Figure 4-10. Furthermore, we describe a generic version of a DRL algorithm designed to learn the intended policy in Algorithm 2 below. For conciseness, the algorithm is presented using the formulation and notation of [ASH22]. The DRL algorithms that will be presented in the next part of this contributions adhere to this general version, although specific details vary depending on the nature and intention of each method.

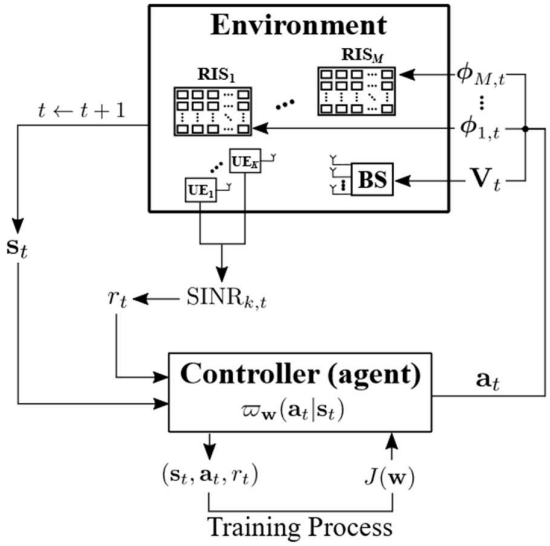

Figure 4-10 Block diagram of the DRL formulation for the sum-rate maximization problem using the system and notation adopted in [ASH22].

Algorithm 2 DRL-Based Training Solving $\mathcal{OP}_1$ in (11)

Require: Number of UEs K, number of RISs M, initial ANN parameters w, policy $\varpi_{\mathbf{w}}$, collection policy $\hat{\varpi}_{\mathbf{w}}$, objective function $J(\cdot)$, final time step T, and update interval t'.

1: **for** $t = 1, 2, \ldots, T$ **do**
2: Estimate $\mathbf{h}_{k,t}$ $\forall k = 1, 2, \ldots, K$.
3: Estimate $\mathbf{H}_{m,t}$ and $\mathbf{g}_{m,k,t}$ $\forall m = 1, 2, \ldots, M$ and $\forall k = 1, 2, \ldots, K$.
4: The controller formulates the state vector $\hat{\mathbf{s}}_t$ similar to (33) using the channel estimates in Steps 2 and 3.
5: The controller decides the action $\mathbf{a}_t$ (i.e., $\phi_{m,t}$ $\forall m$ and $\mathbf{V}_t$) using its policy $\hat{\varpi}_{\mathbf{w}}(\mathbf{a}_t|\hat{\mathbf{s}}_t)$ and shares these settings with the RISs and BS.
6: Each UE_k measures $\text{SINR}_{k,t}$ and sends it to the controller.
7: Using Step 6, the controller computes the reward r_t and stores the experience tuple $(\hat{\mathbf{s}}_t, \mathbf{a}_t, r_t)$ to a set $\mathcal{D}$.
8: **if** $\text{mod}(t, t') = 0$ **then**
9: The controller uses $\mathcal{D}$ to compute $\mathbf{w}^*$ that optimizes $J(\mathbf{w})$.
10: It then performs the updates $\varpi_{\mathbf{w}} \leftarrow \varpi_{\mathbf{w}^*}$ and $\hat{\varpi}_{\mathbf{w}} \leftarrow \hat{\varpi}_{\mathbf{w}^*}$.
11: **end if**
12: **end for**
13: **return** Learned policy $\varpi_{\mathbf{w}}$.

Results and outcomes

A. A novel contextual-bandits DRL algorithm for RIS configurations was proposed: Typically, in RL problems, the *Markov Decision Process* [ASH22] framework is adopted which has resulted in state-of-the-art algorithms like Deep Q Networks (DQN). For the RIS-based problem at hand, it is demonstrated [ASH22, SAH22] that the problem can be cast to a *Contextual Bandits* formalism, which is easier to solve. Motivated by that observation, we proposed a novel DRL-based agent that is tasked to predict the expected reward for all available actions given a state observation, so that the optimal action can be selected.

The performance of the proposed method is depicted in Figure 4-11.The rates are normalized with respect to the optimal achievable rate (obtained by exhaustively searching all configuration and precoding combinations). Both DRL methods greatly outperform the random baseline and achieve near-optimal performance, especially in smaller RIS sizes. DQN and the proposed Neural ϵ-greedy achieve similar results but the Contextual Bandits has smaller computational requirements (DQN requires an effectively double capacity neural-network). The benchmark scheme is discussed below.

B. The effectiveness of a naive but CSI-free Multi-Armed Bandits was examined: A relaxed version of the Contextual Bandits problem, referred to as *Multi-Armed Bandits,* is designed to learn action selection strategies without the need of state observations – relying only on the reward feedback. For the considered task, this has the effect that this control methodology does not rely on any CSI estimation, which greatly reduces the complexity of the network [ASH22]. We have utlised the Upper Confidence Bound (UCB) algorithm which keeps track of a running

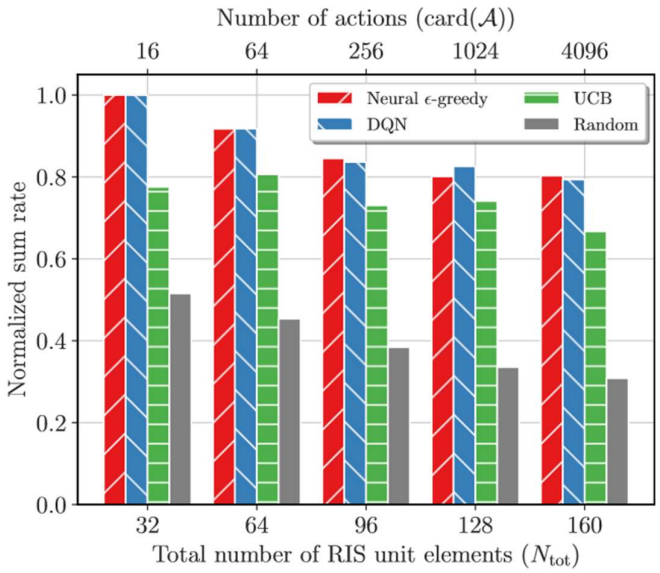

Figure 4-11 Normalized sum rates of the two DRL methods, UCB, and random baseline for the sum-rate maximization objective.

average of the expected reward per action along with a confidence interval. Comparing its performance in the same setup as the aforementioned DRL algorithms (Figure 4-11), it can be seen that this method performs reasonably close to state-of-the-art deep learning approaches, despite its simplicity, offering a great proposition of value in simplified setups. Nevertheless, its performance is expected to decrease in more demanding cases.

C. The problem of tuning large-scale RISs with DRL was investigated: In the above RL formulation, each available RIS configuration is treated as a separate action. When considering quantized phase shift hardware architectures, the cardinality of the action space grows exponentially with the number of unit elements, which imposes severe practical limitations on the size of the RISs than can be effectively controlled. Motivated by the fact that the predominant surface manufacturing processes result to 1-bit quantized RISs:

1. We first deviate from the RL formulation so that we allow for the agents to select the phase shift of each individual RIS element independently, instead of deciding on the complete configuration. By denoting with N the number of RIS elements, this entails taking N binary decisions (which can be viewed as an N-sized binary vector) at each time step, rather than evaluating 2^N possible configurations, which greatly reduces the search space of the problem.
2. We next present two extensions of state-of-the-art DRL algorithms that are specifically designed to deal with binary vectors as actions [SA22]. The first involves approximating the Q function in the DQN algorithm using neural network layers that operate specifically on binary vectors. The maximization step performed by DQN then corresponds to a per-element activation/suppression operation. The network is illustrated in Figure 4-12. The second variation entails applying a discretization operation at the output of the Deep Deterministic Policy Gradients (DDPG) algorithm. DDPG has been designed for problems where the action space consists of continuous vectors. To that end, we have added a post-processing step that maps positive and negative values of the action vector to each of the two available phase shifts of the RIS.

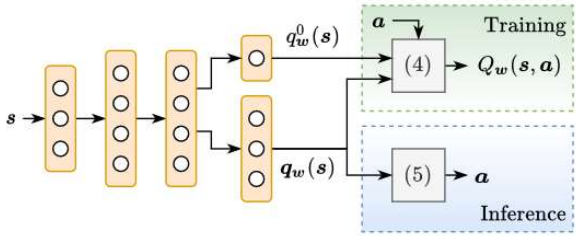

$$Q_{\boldsymbol{w}}(s,a) = q_{\boldsymbol{w}}^0(s) + \sum_{i=1}^{N} [\boldsymbol{a}]_i [\boldsymbol{q}_{\boldsymbol{w}}(s)]_i = q_{\boldsymbol{w}}^0(s) + \boldsymbol{a}^T \boldsymbol{q}_{\boldsymbol{w}}(s). \tag{4}$$

$$[\boldsymbol{a}]_i = \begin{cases} 1, & [\boldsymbol{q}_{\boldsymbol{w}}(s)]_i > 0 \\ 0, & \text{otherwise} \end{cases}, \quad i = 1, 2, \ldots, N. \tag{5}$$

Figure 4-12: Structure and operation of the Q network employed by the proposed extension of the DQN algorithm, termed bin-DQN [SA22]. The Q function is approximated through (4) and the best action vector (i.e. phase shift for each element) can be derived in closed form through (5).

The performance of the proposed methods is depicted in Figure 4-13 for RIS sizes of up to 1500 elements. Since it is infeasible to evaluate traditional RIS tuning methods in such large search spaces, non-optimized, randomly configured RISs were considered as a baseline. It can be inferred, that while the performance of the DRL methods exhibits a decreasing trend, both of those methods offer increased performance in moderate RIS sizes, while DDPG is able to consistently outperform the baseline in all experiments. This decreasing trend in the performance illustrates that the utilised method was not able to achieve satisfactory

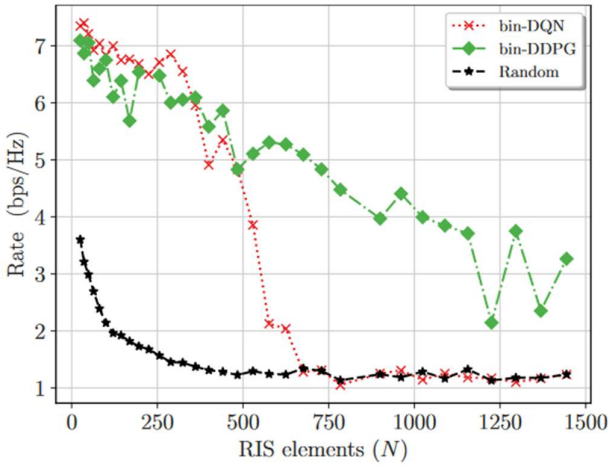

Figure 4-13: Performance of the modified DRL methods (bin-DQN and bin-DDPG) in very large RIS sizes, where other RIS tuning methods are infeasible.

convergence. We attribute this behaviour to the fact that both the size of the neural networks used and the training period were purposely restrained and set to equal values for all experiments. This decision was taken to meet the computational demands of repeating the evaluation process in all different cases, despite the fact that it is expected that the computational resources should grow to meet the demands of the enlarged decision spaces in the more extreme cases. Note that the problem of finding a suitable RIS configuration when

the number of (discrete) unit elements becomes large remains, in large, untreated, and that naively configuring the RIS at random leads to an exponentially decreasing performance.

D. A Multi-hop RIS system has been investigated to combat the strong non-LOS attenuation in the THz bands: Since THz signals suffer from severe propagation attenuation and absorption effects, a system with multiple RISs is envisioned so that the signal arrives at the end user after experiencing multiple RIS-to-RIS reflections. To orchestrate the system, the DDPG algorithm was employed to centrally decide on the cooperative beamforming of all the RISs (infinite resolution phase shifts were assumed) [HYA20]. The performance of the proposed method and system is illustrated in Figure 4-14. The DRL method with multiple hops is able to outperform the benchmark approaches in terms of the total throughput when larger distances are involved. The performance of the system was also examined under different number of BS antennas, RIS elements, and end-users for the two-hop case. It is highlighted that larger RISs can facilitate larger numbers of users.

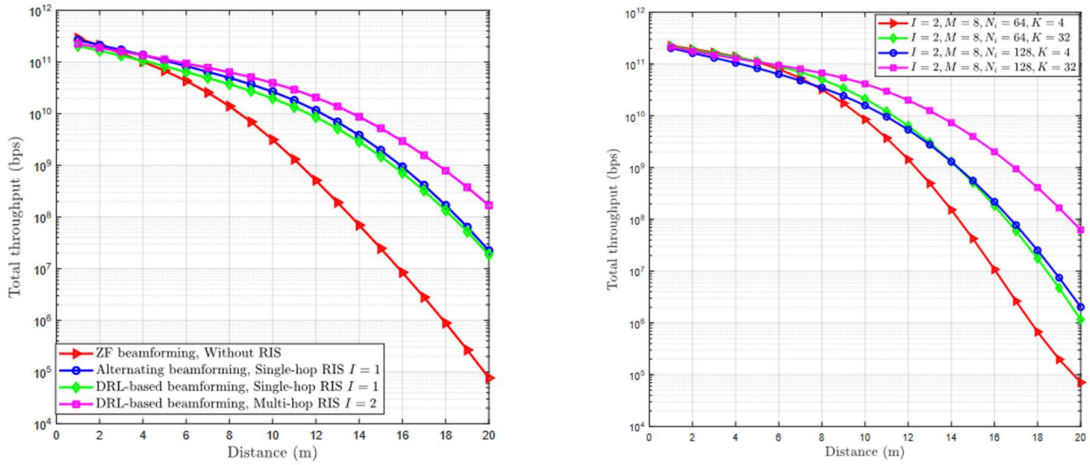

Figure 4-14: Performance of the proposed DRL multi-hop scheme. Notation follows that of [HYA20]. (Left) Zero Forcing (ZF) precoding without RIS and alternating RIS beamforming were selected as benchmarks. (Right) Behavior of the system under different parameters (number of hops, number of BS antennas). number of RIS elements, and number of users).

Perspective and relation to other WP4 contributions

The family of methods of this contribution are suitable for RIS control in wireless environments where the channel states change over time, by leveraging the adaptability and real-time decision making benefits of DRL. The operation of such schemes relies on accurate and fast channel estimation techniques, such as the ones proposed in this deliverable.

4.4.5 Contribution #B-4: Supervised learning of optimal phase configuration based on user positions

Motivation and context

In order to perform RIS beamforming, the RIS(s) phase configuration(s) must be optimized. The optimal configuration depends heavily on the position of the Receiver (RX) at a given time since

the beam(s) must be directed toward it. When the RX changes its position, the optimization procedure must be performed anew, which may be costly operation (in terms of computational resources), especially when multiple RISs are involved. Under this view, the wireless system would benefit from a learning mechanism that is designed to interpolate optimal RIS phases to given RX positions, based on previously observed positions and optimal solution pairs.

Methodology

A deep learning approach is utilised to train Deep Neural Networks that are designed to predict the optimal configuration for given 3D RX coordinates [ASB20]. The system under consideration, depicted in Figure 4-15, is a downlink communication example with includes multiple RISs, in which the TX-RX link is attenuated due to the presence of a blocker. The RX is assumed to be able to move freely inside the designated area. Before the training phase, the data set is constructed by sampling RX positions and solving the multi-RIS rate optimization problem using random channel realisations. When the solution is attained, the position-configuration tuple is stored as a single data point in the training set. The same process is repeated to construct the test set. The DNN receives the position as input and outputs a predicted configuration. The mean squared error between the optimal and predicted configuration is used as the network's loss function.

The interested reader can refer to [ASB20] for all the details on the system model, problem formulation, and algorithmic solutions.

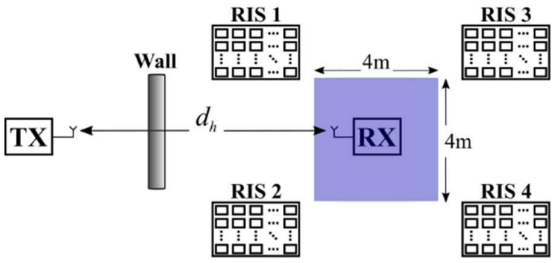

Figure 4-15: The downlink communication system considered for supervised learning of optimal configuration learning.

Results and outcomes

Three different setups are selected for the evaluation process, the first two without the presence of the wall/blocker. The proposed methodology was examined both as a centralized approach (i.e. a common DNN that predicts the configuration of all RISs) and as individually deployed networks onto the RIS controllers (each one controlling its own RIS). As an upper bound, the same training process were repeated, although the networks were now received the channel realisations as inputs, instead of the positions. The results are depicted in Figure 4-16, in terms of the average normalized rate (over the optimal rate of exhaustively solving the optimization problem every time) over the training set. It can be observed that in all cases, the DNN-based methods are able to attain near-optimal performance in the setups considered. When the blocker is not present, the high-quality information of the channel knowledge does not give any significant advantage. Conversely, in the highly attenuated direct link of Setup 3, it is illustrated that the knowledge of the exact CSI can be utilised by the deep learning algorithm to achieve

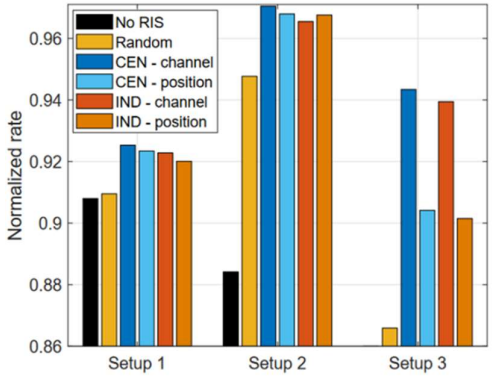

Figure 4-16: Evaluation process of the supervised learning algorithm for predicting the optimal RIS configuration. The networks receive as input either RX position data or channel information. Two variations are considered: (i) A centralized approach where the neural network controls all the surfaces and (ii) an individual approach where each RIS includes its own neural-network based controller. The baselines include selecting the RIS configurations at random and not utilizing any RISs (when the direct link is present).

higher quality rates, rather than position-only inputs. In all cases, the individual and centralized approaches compared equally.

Perspective and relation to other WP4 contributions

The proposed method of this contribution has the advantage of requiring low computational requirements during deployment phase (performing inference on neural networks is substantially less demanding than training), albeit with the extra overhead of the data collection step prior to the deployment phase. Note however, that the operation relies heavily on accurate position estimation of the RX, which is the focus of Work Package 5 of this project. A limitation of this study is its adaptability to changes in the channel states through time. In such cases, the contribution that is based on reinforcement learning may be preferred, although the computational cost is higher.

4.4.6 Contribution #B-5: Reconfiguration of the physical layer for multi beamforming

Motivation and context

Recent works have proven that the operation of the RIS can be tuned during and after deployment. This is achieved by introducing tunable or switchable electronic components within the unit cells and adding appropriate means of control to achieve (re)programmability. Such complexity can often lead to uneconomical designs and fabrication processes, which is an obstacle towards commercializing the applications within 5G networks, such as for Vehicle-to-everything communications (V2X). One way to justify the costs for utilizing RISs in use-cases as pervasive as V2X (which is a form of multi-receiver communication via a single transmitter) is to optimize their operation. To this end, we note that RIS can actually perform multiple functions concurrently, so one design can serve several purposes. Consequently, multi-receiver communication scenarios present a very compelling use case. In a multi-receiver communication scenario, the broadcast station should adequately radiate electromagnetic waves toward the location of the receivers. A wide beam radiation pattern can provide such a requirement. However, a wide beam is detrimental as it radiates energy over a huge space. This strategy is not feasible for mmWave spectrum due to the high propagation losses and blocking effects. The proper solution is to engineer the radiation pattern with respect to the location of the receivers. Hence, independent control on the multiple beams is required.

Methodology

One way to engineer a multi-beam radiation pattern is to control both amplitude and phase (amp/phs) reflection of the unit cells, but since amplitude reconfiguration increase the overall loss, this is not an efficient approach. Another solution is to switch between the users in the time domain, i.e., time division multiplexing (TDM). However, satisfying the 5G key performance indicators (KPIs) for latency renders the TDM approach inefficient. Additionally, dividing RIS area i.e., space division multiplexing (SDM), to engineer the wavefront for multiple beam objective requires a very large RIS. Unlike previous methods that require amplitude reflection control as well as phase reflection control of the unit cells, our proposed strategy requires phase reflection reconfiguration only [TTM22, TJA22]. With this approach the MS realizes multiple-beam radiation pattern with independent control of the beams. Based on realistic system parameters, we then evaluate the performance of the proposed framework by analyzing the throughput for indoor and outdoor scenarios, given the broadcast mode of operation. Note that, the broadcast scenario also entails the multicast scenario, which can be utilized by the radio source to communicate with multiple receivers at the same time. We compare our results to the baseline system and show that by taking advantage of the RIS, a considerable increase in the overall system throughput can be experienced. By considering the energy conservation law, in a closed system, the total energy from the impinging waves should be equal to the energy carried by the scattered beams. Then, there must be an optimal reconfiguration profile with phase-only control by which we can engineer the desired multi-beamforming.

$$\sum_{k=1}^{K} A_{mnk} e^{\Phi_{mn}(\theta_{rk},\phi_{rk})} = 1\ e^{j\Psi_{mn}}$$

where $\Phi_{mn}(\theta_{rk},\phi_{rk})$ is the phase gradient of mn unit cell for the kth-beam aiming the position of the users with reflection angle (θ_{rk},ϕ_{rk}) and K is the number of users. The simplest solution to satisfy equation (above) is to assume all of the beam amplitude are identical $A_{mnk} = A_{mn}$; $k \in [1,K]$. Then we can define this coefficient as the absolute value of the phase gradient summations.

$$A_{mn} = \frac{1}{|\sum_{k=1}^{K} e^{\Phi_{mn}(\theta_{rk},\phi_{rk})}|}$$

Assuming small unit cell size $(D_u < \lambda/2)$, surface current distribution on each unit cell is approximately uniform. Based on Huygens principle, we can assume each unit cell a point source. The total scattering field can be regarded as the superposition of the scattering wave from each unit cell

$$E(\theta,\phi) = \sum_{n=1}^{N}\sum_{m=1}^{M} e^{jk_0\zeta_{mn}} A_{mn} \sum_{k=1}^{K} e^{\Phi_{mn}(\theta_{rk},\phi_{rk})}$$

Now by using above equations, we can implement a multi-beam radiation pattern.

Results and outcomes

Figure 4-17, shows the radiation pattern and relative phase gradient of a square RIS with lateral size of $D_m = 8\lambda$, unit cell size of $D_u = \lambda/3$ and 8 number for the valid states $(0, \pi/4, \pi/2, 3\pi/4, \pi, 5\pi/4, 3\pi/2, 7\pi/4)$.

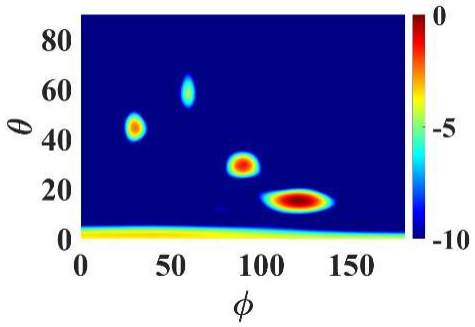

Figure 4-17: Normalized E-field distribution in logarithmic scale (dB) radiating with 4 beams at arbitrary positions with 8 states.

Perspective and relation to other WP4 contributions

To take full advantage of RIS technology and provide significant performance improvements for wireless networks, a proper reconfiguration of the reflection coefficients of unit cells is required. In this work, we propose an efficient reconfiguration technique providing control over multiple beams independently. Compared to time-consuming optimization techniques, this strategy utilizes an analytical method to configure the unit cells for multi-beam radiation. This method is easy to implement, effective and efficient since it only requires phase reconfiguration.

5 Design of Multi-User Techniques for RIS-Empowered Mobile Edge Computing

Mobile edge computing (MEC) represents one of the main technological enablers of 6G networks, which are envisioned to provide a plethora of new services (including verticals), such as Industry 4.0, Internet of Things (IoT), and autonomous driving, building on the tight integration of communication, computation, learning, and control. In this scenario, the goal of MEC is to move cloud functionalities (e.g., computing and storage resources) at the edge of the wireless network, enabling UEs to offload heavy computational tasks to nearby processing units or ESs with the aim of reducing energy consumption and/or service latency [BSD14]. Also, among the many possible applications envisioned by 6G, there is now a huge interest from several research communities in performing distributed, low-latency and reliable edge learning, in which every UE has access to a tiny fraction of the data and low-latency inference/training are performed collectively and distributively at the wireless network edge [MDB21]. However, moving toward millimeter wave (mmWave) communications (and beyond), poor channel conditions due to mobility, dinamicity of the environment, and blocking events, might severely hinder the performance of MEC systems. In this context, a strong performance boost can be achieved by empowering MEC systems with RISs, with the aim of enabling applications running at the edge of the wireless network with the required quality of service in terms of latency, energy, and accuracy. The overall system must then be designed in order to jointly optimize the network resources by dynamically allocating transmission and computational parameters, i.e., rate and clock frequencies, as well as the RIS reflectivity parameters. The goal of this section is to summarize and describe the main achievements of the RISE-6G project in this context.

5.1 Contributions from RISE-6G

The main contributions made by RISE-6G in the design of RIS-empowered MEC are listed below in Table 5-1.

Table 5-1: Main architectural characteristics: Contributions from RISE-6G

Architecture	C-0: Joint optimization and scheduling of communication and computation resources for RIS-empowered Mobile Edge Computing	C-1: RIS-empowered Mobile Edge Computing over intermittent mmWave links	C2: Adaptive federated Learning empowered by Reconfigurable Intelligent Surfaces	C3: Dynamic computation offloading over frequency-selective RIS-empowered communications
# BS	1	1	1	1
# RIS	multiple	1	multiple	1
# UEs	multiple	multiple	multiple	1
Channel and data arrivals acquisition	dynamic	dynamic	dynamic	dynamic
Frequency band	any	mmWave	any	any
LoS/NLoS	LoS	both	LoS	LoS
KPI	Min weighted Energy under service Delay constraint	Min tx Power under service Delay constraint	Min Energy under Delay, Accuracy and Reliability constraints	Min Power under Delay and Reliability constraints

5.1.1 Contribution #C-0: Joint optimization and scheduling of communication and computation resources for RIS-empowered Mobile Edge Computing

Motivation and context

In this section, we propose a dynamic computation offloading algorithm for RIS-empowered MEC. We assume an application that continuously generates data to be offloaded to an ES for processing, e.g., video streaming for anomaly detection. The problem is to enable dynamic computation offloading with minimum energy expenditure, while guaranteeing strict delay constraints dictated by the application running at the ES. To this aim, we have formulated a long-term optimization problem aimed at adaptively allocating radio resources of multiple edge devices and an AP, together with computational resources of an ES and reflectivity parameters (i.e., phase shifts) of multiple RISs [DMC21]. The aim of this algorithmic framework is to reduce the long-term average energy spent by all the network entities (i.e., UEs, AP, ES, and RISs), while guaranteeing a long-term constraint on the average end-to-end delay, computed as previously expressed in Section 2.1 for dynamic computation offloading. To this scope, we define a weighted system energy function given by:

$$e_{\sigma}^{\text{tot}}(t) = \sigma \sum_{k=1}^{K} e_k(t) + (1-\sigma)\left(e_c(t) + e_a(t) + \sum_{i=1}^{I} e_i^r(t)\right)$$

where $e_k(t)$ is the energy spent by each user k to upload data to the AP, in order to enable the task offloading; $e_c(t)$ is the energy consumed by the ES to process data; $e_a(t)$ is the energy that the AP consumes to exchange data with the server, either if is in sleep or in active mode, $e_i^r(t)$ represents the energy spent by the i-th RIS. Finally, $\sigma \in [0,1]$ is a weighting parameter to be chosen, which enables to tune the optimization toward a pure UEs-centric strategy (i.e., $\sigma = 1$), a pure network-centric strategy (i.e., $\sigma = 0$), or a holistic system design (i.e., $\sigma = 0.5$).
Also, we consider a MEC system endowed with I passive RISs, where the i-th RIS is composed of N reflecting elements. In the sequel, we will use the overline notation for uplink parameters,

and the underline notation for downlink. Then, letting $\boldsymbol{\Phi}(t)$ be the vector collecting the phase shifts of all RISs in the system, and assuming a Single Input Single Output (SISO) communication system, the uplink transmission rate between user k and the AP reads as

$$\overline{R}_k(t) = \overline{B}_k \log_2(1 + \overline{a}_k(\boldsymbol{\Phi}(\mathrm{t}))\overline{p}_k(t))$$

for all $k \in \{1, \dots K\}$, where:

$$\overline{\mathrm{a}}_{\mathrm{k}}(\Phi(\mathrm{t})) = \frac{|\,\overline{\mathrm{h}}_{\mathrm{k}}^{\mathrm{a}}(\mathrm{t}) + \sum_{i=1}^{I} \overline{\boldsymbol{h}}_{k,i}(t)^T\, diag(\Phi_i(t))\, \overline{\boldsymbol{g}}_{k,i}^{a}(t)|^2}{\mathrm{N}_0\, \overline{\mathrm{B}}_{\mathrm{k}}}$$

is the RIS-dependent normalized uplink channel coefficient, $\bar{p}_k(t)$denotes the power transmitted by user k at time t, and $\bar{h}_k^a(t)$ represents the direct uplink channel coefficient between user k and the AP; whereas, $\bar{h}_{k,i}(t)$ and $\bar{g}_{k,i}^a(t)$ are vectors containing all the uplink channel coefficients between user k and RIS elements, and between RIS elements and the AP, respectively. Similar expressions hold also for the downlink channel from the AP to the UEs.

Methodology

Leveraging Lyapunov stochastic optimization, the long-term stochastic formulation is solved using a sequence of simpler deterministic problems of the form [DMC21]:

$$\begin{aligned}\min_{\boldsymbol{\Psi}(t)\in\tilde{\mathcal{X}}(t)} \quad & \sum_{k=1}^{K} \Big[\big(Q_k^r(t) - Q_k^l(t) - Z_k(t)\big)\tau \overline{R}_k(t) \\ & + \big(c_k Q_k^a(t) - Q_k^r(t) - Z_k(t)\big)\tau f_k(t) J_k \\ & - \big(Q_k^a(t) + Z_k(t)\big)\tau \underline{R}_k(t) \Big] + V \cdot e_{\sigma}^{\mathrm{tot}}(t)\end{aligned}$$

The first part of the objective function involves several terms related to the service latency, which depends on uplink and downlink rates (i.e., $\bar{R}_k(t)$ and $\underline{R}_k(t)$) and ES CPU clock frequencies $f_k(t)$, weighted by the queue terms $Q_k^r(t)$, $Q_k^l(t)$, and $Z_k(t)$ used to control the long-term delay constraint. The second term of the objective is the weighted system energy previously introduced, multiplied by a parameter V that must be properly chosen. Thus, in a very natural way, the solution of the deterministic problem implements a trade-off between energy and latency that can be tuned using the control parameter V.
Interestingly, the optimization problem can be split into sub-problems to be solved during the first portion of each time slot (as explained in D4.1, section 3.3.5). Then, the overall procedure for the proposed RIS-empowered dynamic mobile edge computing is performed as follows:

1. Perform a greedy optimization to find the RISs phase shifts, aiming at selecting in an iterative fashion the phase shift of the RIS reflective elements that maximize data transmission (in both uplink and downlink).
2. Allocate the optimal uplink transmission power with closed form solutions and optimal downlink powers either with closed form solutions or a water-filling like algorithm.
3. Evaluate if the state of the AP should be in sleep or in active mode, based on an objective function of previously optimized resources.
4. Compute the optimal CPU scheduling through the solution of a linear problem, requiring maximum a few iterations equal to the number of involved devices.
5. For the rest of the time slot, perform the computation offloading or required tasks and then update physical and virtual queues.

The interested reader can refer to [DMC21] for all the details on the system model, problem formulation, and algorithmic solutions.

Results and outcomes

To illustrate the potential advantages introduced by the proposed methodology, we consider a scenario composed by 5 edge devices, 1 AP and 2 RISs with 100 elements each. We assume that an obstacle obscures the direct communication between the UEs and the AP, with an additive path loss attenuation equal to 30 dB. In Figure 5-1 (left), we illustrate the E2E delay as a function of the average energy spent by the overall system, for different scenarios: i) without RIS; ii) with 1 or 2 RIS and for block or full optimization (meaning the phase shift are optimized per group or each of them). The curves are obtained by increasing the Lyapunov trade-off parameter V from right to left. By increasing V, each curve reaches a different value of the energy consumption, while converging to the desired delay bound (equal to 50 ms). As expected, all scenarios with RISs outperform the scenario without RIS in terms of energy-delay trade-off, with the full optimization (with both 1 and 2 RISs) achieving the largest gain. Also, we consider a sub-optimal RIS optimization procedure that divides the RIS in sub-block and associates the same phase shift within the block. Clearly, the block optimization (with Nb = 25 and Nb = 50) reduces complexity at the cost of increased energy with respect to the full strategies. Finally, we explore the performance in terms of energy consumption in the user-centric case ($\sigma = 1$), by varying the number of blocks N_b and the number of bits b_i used to optimize RIS's phases. To this aim, in Figure 5-1 (right), we illustrate the energy consumed by UEs as a function of the number of blocks N_b. As expected, by increasing the number of blocks, the energy consumption decreases thanks to the larger degrees of freedom in optimizing the RISs. Also, increasing the number of bits yields a further reduction in the energy consumption.

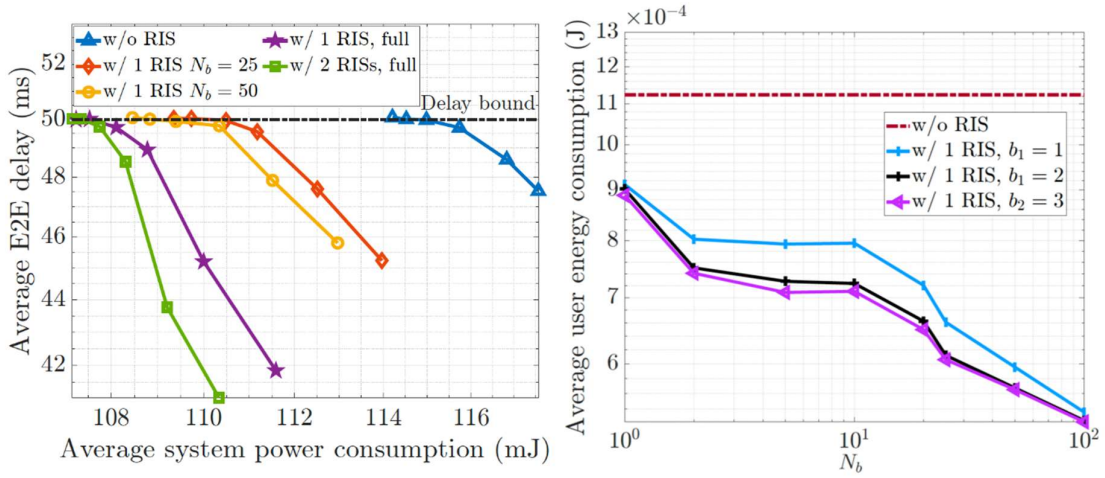

Figure 5-1: (Left) Average E2E delay versus Average system energy consumption, for different scenarios. (Right) Average user Energy consumption versus number of blocks composing the RIS, for different number of quantization bits.

Perspective and relation to other WP4 contributions

The method allows for several generalizations, spanning from the incorporation of sophisticated RIS channel models to the definition of the specific applications running at the edge server. The method hinges on the RIS channel estimation methods developed in WP4.

5.1.2 Contribution #C-1: RIS-empowered Mobile Edge Computing over Intermittent mmWave Links

Motivation and context

In this section, we explore how RISs can assist MEC in overcoming the inherent problems towards high-reliable 6G wireless networks. Then, building on the promising convergence of RISs and MEC, we mainly focus on a joint optimization of radio and computing resources, down to the wireless propagation environment properties. We propose a dynamic optimization algorithm that tackles jointly communication and computation aspects. To this end, we formulate the communication edge computing problem as a long-term optimization aiming to minimize the average users' transmit power, under MEC service delay constraints. We develop this algorithm for a multi-user MIMO (direct and RIS-aided) system by jointly selecting uplink user precoding, RIS reflectivity parameters, and computation resources at a ES collocated at the AP serving the users. For this purpose, we investigate the problem based on a weighted sum of the E2E channel matrix, for each user. Weights are representing two blocking state factors (equals 1 if the direct (indirect) link experiences a blockage event). These factors are respectively related to direct channel between the user and the AP and to the indirect link (comprising the channel between the user and the RIS, and the channel between the RIS and the AP):

$$\boldsymbol{H}_k = \left(1 - \beta_{k,a}\right)\boldsymbol{H}_{k,d} + \left(1 - \beta_{k,r}\right)\boldsymbol{H}_{r,a}\,\boldsymbol{\Phi}\,\boldsymbol{H}_{\boldsymbol{k},\boldsymbol{r}}$$

Then, obviously, the data rate experienced by each user is computed with the blocking weighted channel:

$$R_k(t) = B_k \log_2 \left|\mathbf{I} + \sigma_k^{-2}\mathbf{H}_k(t)\mathbf{Q}_k(t)\mathbf{H}_k^H(t)\right|$$

where $Q_k(t) \in C^{K\times K}$ is the precoding covariance matrix of user k at time t, with K being the number of antennas per user and W_k denotes the bandwidth assigned to user k.

Methodology

The optimization problem is held for the typical case of computation offloading, i.e. the Uplink traffic. Thanks to Lyapunov stochastic optimization, we rigorously transform the original long-term problem into a per-slot problem, thus defining an instantaneous surrogate objective that, in the long-term, guarantees the desired performance:
The overall proposed dynamic resource allocation procedure is described in Algorithm 1.

Algorithm 1 Dynamic optimization of RIS-assisted MEC

Require: $V, \mathcal{U} = \{1, \ldots, N\}$ N_{slots}, τ, P_k^{max}, $B_{l,k}(0)$, $B_{r,k}(0)$, J_k, $\forall k \in \mathcal{U}$, $f_{\max}$,
for $t = 1 : N_{slots}$ **do**
step 1: Optimize $\{\mathbf{Q}_k(t)\}_k$ and $\mathbf{r}(t)$.
  for $n = 1 : I_{\max}$ **do**
step 1.1: $\mathbf{r}^{n+1} = P_\Theta(r_n - \rho \nabla_{\mathbf{r}} f(\mathbf{r}^n, \{\mathbf{Q}_k^{(n)}\}_k))$
step 1.2:
    for $k = 1, \ldots, N$ **do**
      a: If $B_{l,k} \leq B_{r,k}$, $\mathbf{Q}_k^{(n+1)} = \mathbf{0}_K$, else
      b: Update optimal $\{\mathbf{Q}_k^{(n+1)}\}_k$ with water-filling
    end for
  end for
step 2: Optimize $\{f_k(t)\}_k$
step 3: Compute $R_k(t), \forall k \in \mathcal{U}$;
step 4: Update $B_{l,k}$ and $B_{r,k}$.
end for

1- The step 1 of the Algorithm involves the radio resource allocation sub-problem including the optimization of user covariance matrices $\{Q_k(t)\}_k$ and RIS parameters $\boldsymbol{r}(t)$ and is formulated as:

$$\min_{\{\mathbf{Q}_k(t)\}_k, \mathbf{r}(t)} \sum_{k\in\mathcal{U}} (V\mathrm{Tr}(\mathbf{Q}_k(t)) - \tau(B_{l,k}(t) - B_{r,k}(t))R_k(t))$$

The problem is solved while building on an alternating optimization strategy that couples a projected gradient step for the RIS parameters, and a water-filling solution for the users′ precoding.

- ✓ The step 1.1 is of low complexity and allows to allocate the optimal $\boldsymbol{r}(t)$ with a projected gradient based closed form solution. The gradient is a weighted sum of different terms (corresponding to different users), where the weights include both communication and computation queues. This naturally introduces a scheduling of the RIS, which is therefore optimized to prioritize users with worse queueing states.

- ✓ The step 1.2 is related to the problem with respect to the uplink covariances, which presents as well less complexity once the RIS configuration was fixed. For a generic user k for which the communication buffer holds upper than that of the computation, i.e. $B_{l,k}(t) > B_{r,k}(t)$, the problem is convex and admits a water-filling based solution.

2- The step 2 involves the computation resource allocation sub-problem through which optimal frequencies are iteratively allocated to each user [AMD22].
3- In the last step, both physical queues, i.e. communication and computation, are updated.

Results and outcomes

We consider a scenario with multiple users aiming to offload their tasks to an ES collocated at the AP serving the users. All channels are generated through the available tool, the open-source SimRIS Channel Simulator.

Name	Symbol	Value
Number of users	N	6
Bandwidth	B	1 Mhz
Carrier frequency	f	28 Ghz
Noise power spectral density	N_0	-174 dBm/Hz
Slot duration	τ	10 ms
Arrival rate		1 Mbps
The user maximum transmit power	P_k^{max}	100 mw
Transmit and receive antennas	N_u and N_a	4
RIS elements	M	64
The maximum available CPU cycle frequency	f_{max}	4.5 Ghz
The number of CPU cycles per bit	J_k	500

Table 5-2 Simulation Parameters.

For comparison purposes, we assume tow reference strategies, **Alg. 1** where instantaneous knowledge of $\beta_{k,a}\epsilon\{0,1\}(\beta_{k,r}\epsilon\{0,1\})$ is assumed and **Alg. 1, statistical** where only a statistical knowledge of the blockage, i.e. the blocking probabilities $\boldsymbol{p}_{k,a}(t) \in [0,1]\big(\boldsymbol{p}_{k,r}(\boldsymbol{t}) \in [0,1]\big)$ is assumed. In this latter, Algorithm 1 is used, but $\beta_{k,a}(t)$ and $\beta_{k,r}(t)$ are replaced by $\boldsymbol{p}_{k,a}(t)$ and $\boldsymbol{p}_{k,r}(\boldsymbol{t})$, for the optimization.

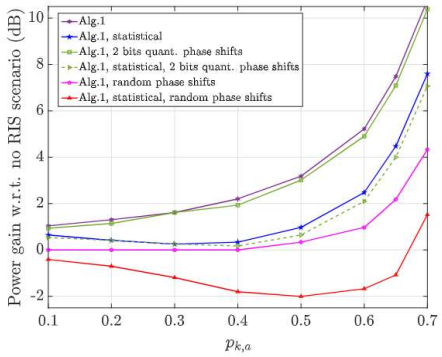

Figure 5-2: Average transmit power versus AP blocking probability

Besides the results presented in section 3.3.5 of D4.1 (Figure 3-15: Delay-Energy trade-off for different strategies), we illustrate in Figure 5-2, the gain in terms of average transmit power of each strategy with respect to the non RIS case, as a function of the direct link blocking, for a fixed E2E delay bound of 150 ms, obtained by tuning the trade-off parameter V. As can be seen, as the blocking probability increases, the gain notably increases with the Alg. 1 strategy, (up to 10 dB for $\boldsymbol{p}_{k,a} = 0.7$), also with quantized phases. Conversely, the gain of Alg. 1, statistical is visible only for higher blocking probabilities, due to the fact that, in this case, the channel knowledge is well-matched to the real channel states. Eventually, this implies that unreliable blocking knowledge is critical for the performance.
Overall, optimizing the RIS through step 1.1 of Algorithm 1 leads to a better exploitation of the indirect path. Therefore, the use of an RIS is prominent to satisfy a reliable MEC-based task offloading in case of bad conditions of the direct link.

Perspective and relation to other WP4 contributions

The investigated tradeoffs will be re-defined while including the control of RIS as discussed and developed in WP4. Also, when practical phase shifts and antenna losses at UEs, AP and RIS are used in such a way investigate the impact of hardware constraints on the results.

5.1.3 Contribution #C-2: Adaptive Federated Learning empowered by Reconfigurable Intelligent Surfaces

Motivation and context

In the context of edge learning, we propose an optimization framework for adaptive federated learning empowered by RISs [BMD22]. The aim of federated learning (FL) is to train a machine learning model (e.g., a neural network) in a distributed fashion at the wireless network edge, where UEs collect data, perform local gradient updates, and then send intermediate estimates to the ES (typically co-located with the AP) that aggregates the local information to provide the final model parameters. An example of RIS-empowered FL scenario is given in Figure 5-3.

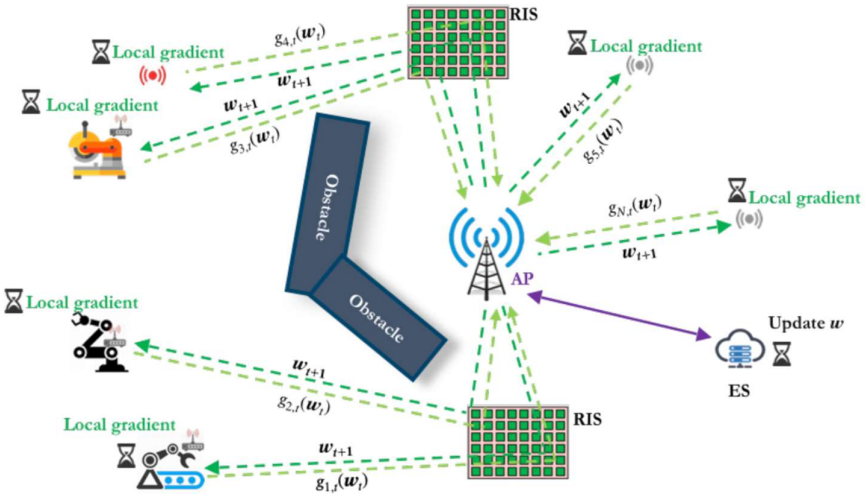

Figure 5-3: RIS-empowered federated learning.

In this setting, it is important that the UE with the best data for the specific learning task can indeed communicate with the ES, to enable good training performance with low-latency updates. However, blocking and variability of the wireless channel could jeopardize the correct behavior of federated edge learning, if not properly handled. In the sequel, we propose to endow federated learning with multiple RISs, with the aim of boosting the training performance in terms of trade-off between the energy spent for learning, the latency required for training, and the accuracy of the final learning task. In particular, the proposed methodology minimizes the long-term average energy consumption of the system, while guaranteeing long-term average constraints on latency, learning performance (i.e., accuracy) and convergence rate. The dynamic algorithm is designed to optimize communication resources (i.e., UEs scheduling, transmission powers, quantization bits), RISs reflectivity parameters, and computation resources (i.e., local and remote CPU frequencies to perform local gradients at the edge devices and global estimation of the learning task at the ES).

Methodology

As a federated learning method, we assumed a distributed stochastic gradient descent (D-SGD) strategy. Then, we model the system power consumption (and the latency needed) for each iteration of D-SGD as the sum of three components: power (and delay) spent to local

computation, power (and delay) needed to upload data from devices to the ES through RIS-empowered links, and power (and latency) to perform estimate aggregation at the ES. These quantities depend on the optimization variables encompassing both communication and computation aspects of the problem. In addition, the proposed method is endowed with an online mechanism that estimates the learning performance and the convergence rate of D-SGD in a totally data-driven fashion. Then, we have formulated a long-term optimization problem aimed at minimizing the long-term average power spent by all the network entities (i.e., UEs, AP, ES, and RISs), while guaranteeing a long-term constraint on the average latency required for training, the average accuracy of the learning task, and the convergence rate of the method. Hinging on Lyapunov stochastic optimization, the problem can be simplified and solved using a sequence of deterministic problems that read as [BMD22]:

$$\min_{\Psi_t \in \mathcal{X}_t} \quad Z_t \widetilde{L}_t - \widehat{Q}_t \widetilde{G}_t - \widehat{Y}_t \widetilde{\alpha}_t + V \cdot p_t^{\text{tot}}$$

where $\tilde{L}_t$, $\tilde{G}_t$, and $\tilde{\alpha}_t$ are the latency, accuracy, and convergence rate metrics at time t, respectively; whereas p_t^{tot} represents the system power consumption weighted by the parameter V. The parameters Z_t, $\hat{Q}_t$, and $\hat{Y}_t$ represent the virtual queues that are used to control and satisfy the long-term constraints. Thus, in a very natural way, the solution of the deterministic problem implements a trade-off between power, latency, and accuracy, which can be tuned using the parameter V.

The solution of the per-slot problem can be performed in two stages:

1. Greedy optimization algorithm to select phase shifts of the RIS, aiming at maximizing RIS-aided channel gains for each communication link, weighted by a factor advantaging devices with the worst direct link with the AP/ES.

2. In the second stage, for each possible training batch size, the method starts from the empty set of transmitting nodes and iteratively adds the most convenient devices, selecting jointly the best number of quantization bits and the associated edge resources computed in closed forms. The method keeps adding devices until the resulting value of the objective function decreases and stops when there is no more incentive in letting other nodes to transmit any bit of information.

The interested reader can refer to [BMD22] for all the details on the system model, problem formulation, and algorithmic solutions.

Results and outcomes

We assess the performance of the proposed method, considering a federated learning task aimed to train a deep convolutional neural network classifier, in a scenario composed by one AP equipped with an ES, 9 UEs, 6 of whom having their direct path to the AP attenuated by an obstacle, and one RIS equipped with 1-bit discrete phase shifters. In Figure 5-4 (left), we show the average uplink power consumption versus the average latency, for different values of average accuracy, comparing the cases where RISs are exploited or not, and a baseline given by an equal-rate with all the agents always transmitting (i.e., no transmission scheduling is implemented). As expected, the trade-off gets worse imposing a stricter requirement on the accuracy, due to the larger power (and number of bits) necessary to obtain the target performance. Also, we can see the gain obtained thanks to the presence of the RIS in the FL task, and the superior performance of the proposed method w.r.t. the baseline.

Finally, in Figure 5-4 (right (a)), we illustrate the temporal behavior of the estimated accuracy of the FL algorithm, obtained for different values of the learning rate α, fixing the accuracy to G = 0.8; also, at time slot 210, we change the accuracy requirement from G = 0.8 to G = 0.9 for the

curve with α = 0.1, introducing a level of non-stationarity. Then, in Figure 5-4 (right (b)), we show the instantaneous latency required by the proposed FL strategy to perform one iteration, together with the latency constraint L = 50 ms. As we can notice, the proposed method is able to obtain the desired learning performance, while controlling the convergence rate, and satisfying the required latency constraint. Furthermore, the method can react promptly to changes in the accuracy requirement, exhibiting powerful learning and adaptation capabilities in a fully data-driven fashion.

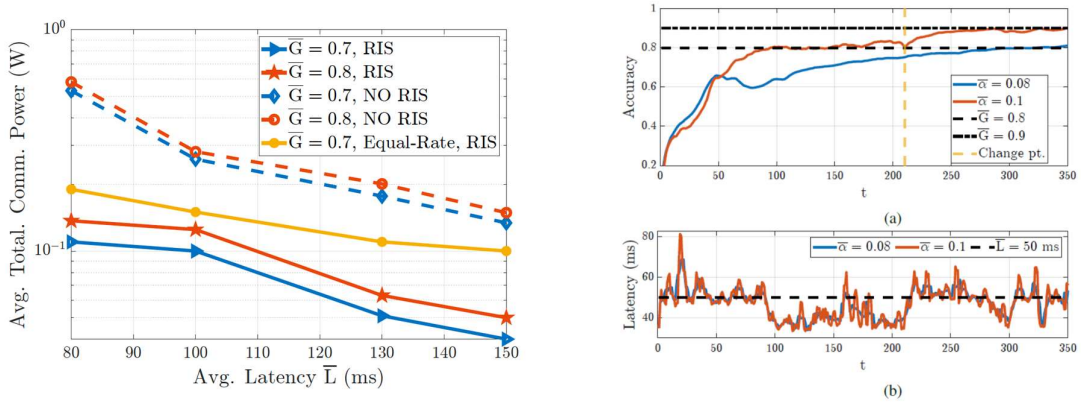

Figure 5-4: (Left) Average communication power versus average delay, for different scenarios and strategies. (Right) (a) Accuracy versus time. (b) Latency versus time.

Perspective and relation to other WP4 contributions

The method allows for several generalizations, spanning from the incorporation of sophisticated RIS channel models to the definition of more general federated training algorithms. The method hinges on the RIS channel estimation methods developed in WP4.

5.1.4 Contribution #C-3: Dynamic Computation Offloading over frequency-selective RIS-empowered communications

Motivation and context

The last contribution [MCK22] of this section focuses on the intersection between the possibility of adapting wireless propagation as per end users' convenience according to specific service requirements, enabled by RISs, and the possibility to bring a powerful distributed computing environment at the wireless edge, enabled by the MEC. In particular, we leverage on the recently developed Lorentzian model for RIS reconfiguration parameters, which allows the optimization of the wireless communication through frequency dependent RIS response profiles. From the user perspective, the goal is to minimize the power spent by the device for processing data locally and then transmit information units in order to enable a desired computation offloading task, within a maximum required service delay. Specifically, for local computation, the user device spent an amount of power: $p_t^l = \gamma \left(f_t^l\right)^3$, experiencing a delay $D_t^l = w_t^l / f_t^l$, where f_t^l is the portion of CPU dynamically allocated to process the workload w_t^l during each time slot. For transmission, let us consider a multi-carrier system with subcarrier spacing W and central frequency f_b on frequency bin $b \in B$, with B the set of bins, and $p_{b,t}$ the portion of the user transmit power dynamically allocated in each bin, under the constraint of the maximum power p_{max} available at the device: $p_t^u = \sum_{b \in B} p_{b,t} \leq p_{max}$. Then, the communication delay is computed as: $D_t^u = A_t / R_t$, where the uplink rate is given by $R_t = W \log_2(1 + \alpha_t(f_b) p_{b,t})$, and the overall channel to noise ratio on frequency bin b can be written as:

$$\alpha_t(f_b) \triangleq \frac{|h_t^{\mathrm{LoS}}(f_b) + \mathbf{g}_t^{\mathrm{T}}(f_b)\mathbf{\Phi}_t(f_b)\mathbf{h}_t(f_b)|^2}{N_0 W}$$

Together with the optimization of radio and computing resources, here we jointly also optimize frequency dispersive aware RIS configuration, i.e. multi-carrier frequency selective RIS elements' responses. We consider the response of each n-th element of the RIS as for a polarizable dipole and then, following the Lorentzian discrete form on subcarrier f_b, we can compute each element of the diagonal matrix $\mathbf{\Phi}$, as:

$$\phi_{n,t}(f_b) = \frac{S_{n,t} f_b^2}{f_{n,t}^2 - f_b^2 + j\frac{f_{n,t}}{2\chi_{n,t}} f_b},$$

where $f_{n,t}, S_{n,t},$ and $\chi_{n,t}$ are the element-dependent oscillator strength, resonance frequency, and quality factor, which can be externally controlled, in each time slot t.

Methodology

We formulate a long-term optimization problem aimed at minimizing the average system power consumption constrained to average latency constraints. Thus, hinging on Lyapunov stochastic optimization, we convert the long-term problem into a sequence of lower complexity deterministic problems, with convergence and asymptotic optimality guarantees with respect to the original problem. More specifically, to deal with long-term constraints, we make use of mathematical models known as virtual queues, able to track the state of the system in terms of constraint violations, to take control actions, thus driving the system towards efficient and reliable operations. Then, the final optimization problem reads as:

$$\min_{\mathbf{\Theta}} \quad \sum\nolimits_{k=1}^{K} \left[V p_t^{\mathrm{tot}} + Y_t D_t^{\mathrm{tot}} + Z_t \mathbf{1}\{O_t\}\right]$$

with $\mathbf{\Theta}_t = [\{f_{n,t}\}_n, \{S_{n,t}\}_n, \{\chi_{n,t}\}_n, \{p_{b,t}\}_b, f_t^l]$. In particular, Y and Z are virtual queues handling delay constraints, on average and probabilistic respectively, for each time slot t. The problem can be then simplified introducing an upper bound and an approximation, and finally split into three sub-problems, with low-complexity and efficient solutions. The main steps of the proposed method are:

a) Solve a convex sub-problem to find optimal speed-clock scheduling f_t^l, for each time slot, in closed-form solution.

b) Solve the optimization of RIS' parameters, through a heuristic algorithm, building on the one proposed in [DMC21], in which RIS elements responses are subsequently selected with the goal of increasing a weighted sum of channel power gains. Here, to deal with frequency selective channels, we propose to subsequently select RIS parameters (i.e. $S_{n,t}$, $f_{n,t}$ and $\chi_{n,t}$) for each element, in order to maximize the sum of the channel power gains over all subcarriers.

c) Given an RIS configuration, we can finally solve a convex problem to find the uplink power allocation over subcarriers $p_{b,t}$, with an efficient algorithm, such as interior-point method.

The interested reader can refer to [MCK22] for all the details on the system model, problem formulation, and algorithmic solutions.

Results and outcomes

We assess the performance of our proposed optimization method through a scenario composed of one user device, one AP and one RIS with 100 elements. Time is divided in slots of equal duration, during each slot Rayleigh fading SISO channels are generated, with 4 delayed taps, and their Fourier transform is performed to obtain the channel transfer functions. We compare the RIS-aided performance with the Lorentzian model and our frequency selective-aware optimization, termed as *Lorentzian RIS*, with two benchmarks: i) the case without the RIS, termed as *no RIS*; ii) the frequency flat RIS case, termed as *flat RIS*, in which the RIS response does not follow the realistic Lorentzian model, but it is flat across all frequencies. In Figure 5-5 (left), we show the trade-off between the average E2E delay and the power consumption, obtained by increasing the parameter V from right to left, for two different average delay thresholds, namely 100 ms and 80 ms, and no probabilistic delay constraint imposed. As we can notice, for all curves, the average E2E delay increases as the power consumption decreases, until approaching the delay constraint. However, the *no RIS* case exhibits the worst performance in terms of delay-power trade-off, as it achieves higher delays for a fixed power consumption. At the same time, the best performance is achieved by the *Lorentzian RIS* (i.e. the proposed method). Moreover, focusing on the highest delay (points on the left side of the plot), which is indeed the service requirement, we can notice how the *Lorentzian RIS* case achieves the lowest power consumption, while a slight gain with respect to the *no RIS* case is achieved by the *flat RIS*. However, the latter does not achieve the considerable gain achieved by the proposed method, due to the awareness of the latter on frequency selective channels and RIS responses. Finally, in Figure 5-5 (right), we plot the complementary distribution function of the delay, also known as survivor function, for the highest value of V, validating the ability of our algorithm to guarantee the probabilistic constraint, as shown by the intersection of the curves between the maximum allowed delay D^{max} and the reliability threshold ϵ.

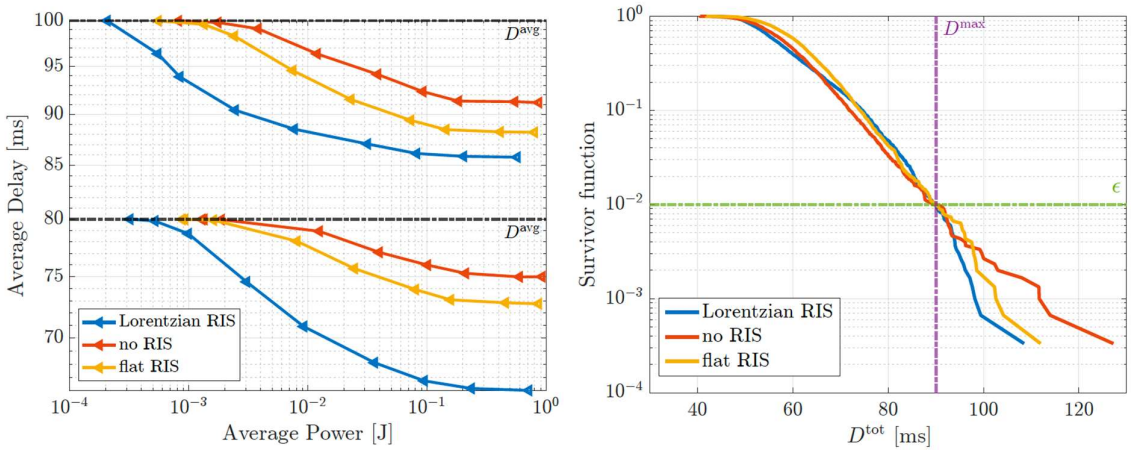

Figure 5-5: (Left) Average power consumption versus average delay, for different strategies. (Right) Survivor function.

Perspective and relation to other WP4 contributions

The method allows for several generalizations, spanning from multi-user and multi RIS scenario to the definition of the specific applications running at the edge server. The method hinges on the RIS channel estimation methods developed in WP4.

6 Conclusions and outlook

In the present deliverable, we have reported major research advances and contributions for each of the three tasks of WP4 under examination. Specifically, the main contributions and takeaways obtained by the RISE-6G consortium can be summarized as follows.

(1) In the context of RIS-aided massive multiple-access cellular networks, we have proposed the RISMA protocol, which is shown to outperform the most advanced and state of the art competing protocols.

(2) In the context of RIS-aided air-to-ground networks, we have proposed an optimization framework that is shown to be robust and effective against several undesired flight effects, and it is capable to offer the desired performance gains.

(3) In the context of developing RIS-aided schemes that can dynamically operate in different frequency bands, we have proposed a novel design of unit cell based on PIN diodes and patch antennas. The proposed solution minimizes the impact of mutual coupling, while not compromising the beamforming gain.

(4) In the context of reducing the channel estimation overhead and ease the deployment of RISs in wireless networks, we have proposed a novel RIS architecture with integrated communication and sensing capabilities, which does not need a dedicated control channel. The proposed approach is shown to provide sum-rate performance close to state of the art CSI-aware solutions.

(5) In the context of developing efficient and scalable optimization methods for RIS-aided networks, we have introduced algorithms based on the theory of quantum annealing and have shown their good performance in muti-user environments.

(6) In the context of developing physically consistent models for RISs that can be integrated into optimization frameworks for communications, we have developed an RIS model based on mutually coupled antennas and have shown that it is suitable for optimizing multi-user RIS-aided networks as a function of the mutual coupling. Thanks to the proposed approach, the mutual coupling can be leveraged to obtain better performance.

(7) In the context of developing efficient ray-based methods, we have reported a proof-of-principle analysis of the efficacy of ray-tracing approaches based on DEA.

(8) In the context of developing efficient and scalable channel estimation methods for RIS-aided networks, we have developed a novel channel estimation procedure that tracks the variations of the wireless channel with minimal channel overhead.

(9) In the context of finding a good tradeoff between performance and channel estimation overhead, we have introduced a new optimization strategy for RIS-aided channels that relies on statistical information about the users' locations rather than on instantaneous CSI. It is shown that the proposed approach offers competitive performance as full-CSI methods but at reduced overhead.

(10) In the context of improving multi-user communications in RIS-aided channels affected by the presence of blocking objects, we have developed a novel random-access protocol and have shown that the deployment of RISs allows for better resolving the access collisions and for increasing the average number of successful access attempts.

(11) In the context of designing efficient and adaptive solutions for RIS-aided networks, we have developed algorithms based on the framework of deep reinforcement learning, and have developed a trainable decision maker that continuously observes the CSI and selects the RIS configurations for system optimization.

(12) In the context of reducing the computational requirements at the deployment phase of RIS-aided networks, we have proposed a deep neural network approach that is capable of predicting the optimal configuration of RISs based on less demanding inferences since the training is performed offline.

(13) In the context of enabling multi-user communications, RISs need to be capable of realizing multiple beams simultaneously. We have proposed an efficient reconfiguration technique that allows the control over multiple beams independently. The method is shown to be easy to implement, effective, and efficient since it only requires phase reconfigurations.

(14) In the context to ease the channel estimation process in RIS-aided networks, we have introduced the concept of frequency-mixing RISs with the objective of reducing the complexity of channel estimation and enabling the estimation of many RIS-aided channels simultaneously.

(15) In the context of designing dynamic computation offloading schemes with minimum energy expenditure and strict delay constraints, we have introduced a dynamic computation offloading algorithm that capitalizes on RISs and MEC.

(16) In the context of designing networks that can jointly support communication and computation tasks, we have introduced a dynamic optimization algorithm that is capable of overcoming the presence of blocking objects and of offering reliable MEC-based task offloading opportunities in the presence of unreliable links.

(17) In the context of developing RIS-aided networks that can quickly adapt to the channel and network conditions, we have introduced an optimization framework based on federated learning and have shown its superior performance compared to state of the art methods.

(18) In the context optimizing RISs that account for the frequency-dependent response of the RIS elements, we have developed an efficient optimization framework to minimize the power spent by the devices for data processing and the transmission to edge servers.

In conclusion, the planned objectives for deliverable D4.2 are all achieved as per the Grant Agreement. The proposed solutions will be consolidated and generalized towards the finalization of deliverable D4.4

References

[A21]	A. Abrardo et al., “Intelligent reflecting surfaces: Sum-rate optimization based on statistical position information,” IEEE Trans. Commun., early access, Jul. 12, 2021, doi: 10.1109/TCOMM.2021.3096549
[ADS22]	A. Albanese, F. Devoti, V. Sciancalepore, M. Di Renzo, and X. Costa-Ṕerez, “MARISA: A Self-configuring Metasurfaces Absorption and Reflection Solution Towards 6G,” in IEEE INFOCOM 2022 - IEEE Conference on Computer Communications, 2022.
[AMD22]	F. Ezzahra Airod, M. Merluzzi, P. Di Lorenzo, and E. Calvanese Strinati, Reconfigurable Intelligent Surface Aided Mobile Edge Computing over Intermittent mmWave Links, accepted for publication to IEEE SPAWC, 2022. Online: https://arxiv.org/abs/2205.15052.

[ASB20]	G. C. Alexandropoulos, S. Samarakoon, M. Bennis, and M. Debbah, "Phase configuration learning in wireless networks with multiple reconfigurable intelligent surfaces," in Proc. IEEE Global Communications Conference, Taipei, Taiwan, 7–11 December 2020, pp. 1–6.
[ASH22]	G. C. Alexandropoulos, K. Stylianopoulos, C. Huang, C. Yuen, M. Bennis, and M. Debbah, "Pervasive machine learning for smart radio environments enabled by reconfigurable intelligent surfaces," IEEE Proceedings, to appear, 2022.
[BMD22]	C. Battiloro, M. Merluzzi, P. Di Lorenzo, and S. Barbarossa, Dynamic Resource Optimization for Adaptive Federated Learning empowered by Reconfigurable Intelligent Surfaces, proc. of IEEE ICASSP, Singapore, June 2022.
[BSD14]	S. Barbarossa, S. Sardellitti, and P. Di Lorenzo, Communicating while Computing: Distributed Mobile Cloud Computing over 5G Heterogeneous Networks, IEEE Signal Processing Magazine, vol. 31, no. 6, pp. 45-55, Nov. 2014.
[CSL22]	V. Croisfelt, F. Saggese, I. Leyva-Mayorga, R. Kotaba, G. Gradoni, P. Popovski, "A Random Access Protocol for RIS-Aided Wireless Communications", accepted for publication to IEEE SPAWC, 2022. Online: https://arxiv.org/abs/2203.03377
[D78]	Dowker, J.S., 1978. “Spectra of Finite Systems: A Review of Weyl's Problem–The Eigenvalue Distribution of the Wave Equation for Finite Domains and its Applications on the Physics of Small Systems,” Phys. Bull. 29 181 (1978).
[DDC20]	L. Dai, M. Di Renzo, C. B. Chae, L. Hanzo, B. Wang, M. Wang, X. Yang, J. Tan, S. Bi, S. Xu, F. Yang, and Z. Chen, “Reconfigurable Intelligent Surface-Based Wireless Communications: Antenna Design, Prototyping, and Experimental Results”. IEEE Access, 8, 45913–45923, 2020.
[DMC21]	P. Di Lorenzo, M. Merluzzi, E. Calvanese Strinati, and S. Barbarossa, “Dynamic Edge Computing empowered by Reconfigurable Intelligent Surfaces,” Online: https://arxiv.org/abs/2112.11269, 2021.
[DMS22]	F. Devoti, P. Mursia, V. Sciancalepore, and X. Costa-Perez, “Taming Aerial Communication with Flight-assisted Smart Surfaces in 6G Era”, 2022, [Online]: https://arxiv.org/abs/2205.08581
[GCT15]	Gradoni, G., Creagh, S.C., Tanner, G., Smartt, C. and Thomas, D.W., 2015. A phase-space approach for propagating field–field correlation functions. New Journal of Physics, 17(9), p.093027.
[GD21]	G. Gradoni and M. Di Renzo, “End-to-end mutual-coupling-aware communication model for reconfigurable intelligent surfaces: An electromagnetic-compliant approach based on mutual impedances,” IEEE Wireless Commun. Lett., vol. 10, no. 5, pp. 938–942, May 2021.
[GDR21]	Gradoni, G., Di Renzo, M., Diaz-Rubio, A., Tretyakov, S., Caloz, C., Peng, Z., Alu, A., Lerosey, G., Fink, M., Galdi, V. and Cui, T.J., 2021. Smart Radio Environments. arXiv preprint arXiv:2111.08676.
[H19]	C. Huang, “Reconfigurable intelligent surfaces for energy efficiency in wireless communication,” IEEE Trans. Wireless Commun., vol. 18, no. 8, pp. 4157–4167, Aug. 2019. [Online]. Available: https://ieeexplore.ieee.org/document/8741198
[HYA20]	C. Huang, Z. Yang, G. C. Alexandropoulos, K. Xiong, L. Wei, C. Yuen, and Z. Zhang, "Hybrid beamforming for RIS-empowered multi-hop terahertz communications: A DRL-based method," in Proc. IEEE Global Communications Conference, Taipei, Taiwan, 7–11 December 2020, pp. 1–6.
[HZA19]	C. Huang, A. Zappone, G. C. Alexandropoulos, M. Debbah and C. Yuen, "Reconfigurable Intelligent Surfaces for Energy Efficiency in Wireless Communication," in IEEE Transactions on Wireless Communications, vol. 18, no. 8, pp. 4157-4170, Aug. 2019, doi: 10.1109/TWC.2019.2922609.
[HZD20]	J. Hu, H. Zhang, B. Di, L. Li, K. Bian, L. Song, Y. Li, Z. Han, and H. V. Poor, “Reconfigurable Intelligent Surface Based RF Sensing: Design, Optimization,

	and Implementation". IEEE Journal on Selected Areas in Communications, 38(11), 2700–2716, 2020
[LRG22]	Q. J. Lim, C. Ross, G. Gradoni, and Z. Peng, "Quantum-Assisted Combinatorial Optimization of Reconfigurable Intelligent Surfaces", 16th European Conference on Antenna and Propagation (EuCAP), Madrid, Spain, 27 March – 01 April 2022. [Best Electromagnetics Paper Award]
[MAM22]	F. Maresca, A. Albanese, P. Mursia, V. Sciancalepore, and X. Costa-Pérez, "A Frequency-Agnostic RIS-based solution to control the Smart Radio Propagation Environment," accepted for publication in 23rd IEEE International Workshop on Signal Processing Advances in Wireless Communications (SPAWC), 2022, [Online]: http://arxiv.org/abs/2203.08633
[MCK22]	M. Merluzzi, F. Costanzo, K.D. Katsanos, G. C. Alexandropoulos, P. Di Lorenzo, Power Minimizing MEC Offloading with QoS Constraints over RIS-Empowered Communications, submitted to IEEE GLOBECOM, 2022.
[MDB21]	Merluzzi, M., Di Lorenzo, P., Barbarossa, S.: Wireless edge machine learning: Resource allocation and trade-offs. IEEE Access 9, pp. 45377–45398, 2021
[MDS21]	P. Mursia, F. Devoti, V. Sciancalepore and X. Costa-Pérez, "RISe of Flight: RIS-Empowered UAV Communications for Robust and Reliable Air-to-Ground Networks," in IEEE Open Journal of the Communications Society, vol. 2, pp. 1616-1629, 2021.
[MSG21]	P. Mursia, V. Sciancalepore, A. Garcia-Saavedra, L. Cottatellucci, X. C. Pérez and D. Gesbert, "RISMA: Reconfigurable Intelligent Surfaces Enabling Beamforming for IoT Massive Access," in IEEE Journal on Selected Areas in Communications, vol. 39, no. 4, pp. 1072-1085, April 2021.
[NKC20]	Q.-U.-A. Nadeem, A. Kammoun, A. Chaaban, M. Debbah, and M.-S. Alouini, "Asymptotic max-min SINR analysis of reconfigurable intelligent surface assisted MISO systems," IEEE Trans. Wireless Commun., vol. 19, no. 12, pp. 7748–7764, Apr. 2020.
[PHS05]	C B Peel, B M Hochwald, and A L. Swindelhurst, "A Vector-Perturbation Technique for Near-Capacity Multiantenna Multiuser Communication - Part I: Channel Inversion and Regularization," IEEE Trans. Commun., vol. 53, no. 1, pp. 195–202, Jan. 2005.
[PSZ21]	X. Pang, M. Sheng, N. Zhao, J. Tang, D. Niyato and K. -K. Wong, "When UAV Meets IRS: Expanding Air-Ground Networks via Passive Reflection," in IEEE Wireless Communications, vol. 28, no. 5, pp. 164-170, October 2021, doi: 10.1109/MWC.010.2000528.
[QD21]	X. Qian and M. Di Renzo, "Mutual coupling and unit cell aware optimization for reconfigurable intelligent surfaces," IEEE Wireless Commun. Lett., vol. 10, no. 6, pp. 1183–1187, Jun. 2021.
[RGL22]	C. Ross, G. Gradoni, Q. J. Lim and Z. Peng, "Engineering Reflective Metasurfaces With Ising Hamiltonian and Quantum Annealing," in IEEE Transactions on Antennas and Propagation, vol. 70, no. 4, pp. 2841-2854, April 2022, doi: 10.1109/TAP.2021.3137424.
[RSA20]	D. Ramaccia, D. L. Sounas, A. Alu, A. Toscano, and F. Bilotti, "Phase-induced frequency conversion and doppler effect with time-modulated metasurfaces," IEEE Transactions on Antennas and Propagation, vol. 68, no. 3, pp. 1607–1617, 2020.
[S65]	Slepian, D., 1965. "Some asymptotic expansions for prolate spheroidal wave functions," Journal of mathematics and physics, 44(1-4), pp.99-140.
[SA22]	K. Stylianopoulos and G. C. Alexandropoulos, "Online RIS configuration learning for arbitrary large numbers of 1-bit phase resolution elements," IEEE International Workshop on Signal Processing Advances in Wireless Communications, Oulu, Finland, 4–6 July 2022, to be presented.

[SAH22]	K. Stylianopoulos, G. C. Alexandropoulos, C. Huang, C. Yuen, M. Bennis, and M. Debbah, "Deep contextual bandits for orchestrating multi-user MISO systems with multiple RISs," IEEE International Conference on Communications, Seoul, South Korea, 16–20 May 2022.
[SRL11]	Q. Shi, M. Razaviyayn, Z.-Q. Luo, and C. He, “An iteratively weighted MMSE approach to distributed sum-utility maximization for a MIMO interfering broadcast channel,” IEEE Trans. Signal Process., vol. 59, no. 9, pp. 4331–4340, Sep. 2011.
[SSH04]	Q. H. Spencer, A.L. Swindlehurst, and M. Haardt “Zero-forcing methods for downlink spatial multiplexing in multiuser MIMO channels”, IEEE Transactions on Signal Processing, 52(2), 461–471, 2004.
[TJA22]	H. Taghvaee, A. jain, S. Abadal, G. Gradoni, E. Alarcón and A. Cabellos-Aparicio, 2022, "On the Enabling of Multi-receiver Communications with Reconfigurable Intelligent Surfaces," arXiv:2106.06789v2.
[TTM22]	H. Taghvaee, S. Terranova, N. M. Mohammed and G. Gradoni, 2022, "Sustainable Multi-User Communication with Reconfigurable Intelligent Surfaces in 5G Wireless Networks and Beyond," 16th European Conference on Antennas and Propagation (EuCAP), pp. 1-5.
[Wid64]	Widom, H., 1964. Asymptotic behavior of the eigenvalues of certain integral equations. II. Archive for Rational Mechanics and Analysis, 17(3), (1964).
[WZ19]	Q. Wu and R. Zhang, “Intelligent reflecting surface enhanced wireless network via joint active and passive beamforming,” IEEE Trans. Wireless Commun., vol. 18, no. 11, pp. 5394–5409, Nov. 2019.
[WZ19]	Q. Wu, and R. Zhang, “Intelligent Reflecting Surface Enhanced Wireless Network: Joint Active and Passive Beamforming Design”, IEEE Transactions on Wireless Communications, vol. 18, no. 11, pp. 5394-5409, Nov. 2019.
[YAK22]	J. Yuan, G. C. Alexandropoulos, E. Kofidis, T. Lindstrm Jensen, E. De Carvalho, “Tensor-based Channel Tracking for RIS-Empowered Multi-User MIMO Wireless Systems,” Online: https://arxiv.org/abs/2202.08315
[YDW21]	J. Yuan, E. De Carvalho, R. J. Williams, E. Björnson and P. Popovski, "Frequency-Mixing Intelligent Reflecting Surfaces for Nonlinear Wireless Propagation," in IEEE Wireless Communications Letters, vol. 10, no. 8, pp. 1672-1676, Aug. 2021, doi: 10.1109/LWC.2021.3077085.
[YXN21]	L. You, J. Xiong, D. W. K. Ng, C. Yuen, W. Wang, and X. Gao, “Energy efficiency and spectral efficiency tradeoff in RIS-aided multiuser MIMO uplink transmission,” IEEE Trans. Signal Process., vol. 69, pp. 1407–1421, 2021.
[YYH20]	W. Yan, X. Yuan, Z.-Q. He, and X. Kuai, “Passive beamforming and information transfer design for reconfigurable intelligent surfaces aided multiuser MIMO systems,” IEEE J. Sel. Areas Commun., vol. 38, no. 8, pp. 1793–1808, Aug. 2020.
[Z20]	M.-M. Zhao, “Intelligent reflecting surface enhanced wireless networks: Two-timescale beamforming optimization,” IEEE Trans. Wireless Comm., vol. 20, no. 1, pp. 2–17, Jan. 2020.